室蘭工業大学
学術資源アーカイブ
Muroran Institute of Technology Academic Resources Archive

# インフルエンザウイルスのサブタイプ判定に用いる局所励起表面プラズモンセンサーの開発に関する研究



| メタデータ | 言語: eng<br>出版者:<br>公開日: 2013-11-15<br>キーワード (Ja):<br>キーワード (En):<br>作成者: 寧, 君<br>メールアドレス:<br>所属: |
|---|---|
| URL | https://doi.org/10.15118/00005106 |

# DEVELOPMENT OF A LOCALIZED SURFACE PLASMON SENSOR FOR THE DETECTION OF INFLUENZA VIRUSES WITH SPECIFIC SUBTYPES

September 2013

---

Jun Ning

Division of Engineering for Composite Functions
Graduate School of Engineering, Muroran Institute of Technology

---

# Acknowledgments

Firstly, I would like to express my deepest gratitude to my supervisor, Dr. Hiroshi Kano at Muroran Institute of Technology, who is responsible and resourceful scholar. He has provided constant encouragement and valuable guidance to me at all of the stages of this thesis. Without his illuminating instructions, this thesis could not reach its present form.

It is also my pleasure to thank Dr. Hideki Hasegawa and Dr. Akira Ainai at National Institute of Infectious Diseases for their kind contribution in the preparation of samples. I would like to express my sincere gratitude to Dr. Koyo Watanabe and Dr. Goro Terakado for valuable discussions and sharing the scientific knowledges, and also thank Mr. Kotaro Nagata and Mr. Issei Wrushihara for helping my experiments.

Lastly, but not least, I would like to thank my family for providing most valuable encouragement throughout the entire project. I greatly appreciate your support.

Jun Ning
Sep. 2013

# Contents

# Chapter 1 Introduction

## 1.1 Detection of biomolecular interactions by using a surface plasmon

Surface plasmon is a quantum of free electron oscillations, which can be excited on a metal surface in particular configurations [1]. This phenomenon was initially found by Wood in 1902 [2]. When metallic diffraction grating is illuminated by polychromatic light, patterns of unusual dark bands in the reflected light are found. This phenomenon is considered as anomalies which gives no clear physical explanation. Until 1957, Rufus Ritchie was the first to predicate the existence of surface plasmons [3]. In 1968, Otto initially excited a surface plasmon using the attenuated total reflection method in a prism coupled structure [4]. In the same year, Kretschmann and Reather reported the excitation of surface plasmons in another configuration of attenuated total reflection method [5].

Nylander and Liedberg demonstrated that a sensing method can be used to detect bimolecular interactions using a surface plasmon excited in the Kretschmann configuration [6–8]. A sensing technique based on the surface plasmons has attached the high attention in the research because of its high sensitivity, fast response, free label and real-time monitoring [9–13]. This technique can be utilized in the medical diagnosis, environmental monitoring, food safety screening, and so on [14–19].

Because the dispersion relation of surface plasmons strongly depends on the refractive index of the dielectric medium which covers the metal surface, they can be used as a sensing probe to measure the refractive index. The sensors have been applied to interactions among proteins, DNA, and some other bio-related molecules [20–26]. In the typical cases, interactions between target molecules (e.g., antigen) and target-recognizing molecules (e.g., antibody) immobilized on the sensing surface are measured as variation of refractive index [27–31]. Characteristics provided by surface plasmon sensing fit well in these applications [32–37].

In the development of these sensors, parallel detection of multiple targets in one measurement is one of the biggest concerns [38, 39]. Since an affordable volume of a sample is often limited in the measurements of biological samples, a parallel detection that uses little sample volume is preferred by most research institutes. To achieve this, a small measurement probe is required. The method to localize surface plasmons on a flat metal surface can produce a sensing volume with an ultra small amount.

The localized surface plasmons on a flat metal surface can be excited by focusing light on the sensing surface of Kretschmann configuration through an objective lens with a high

numerical aperture [40–43]. In this case, surface plasmons propagating in many directions can be excited coherently. These surface plasmons interfere with one another to localize in the microscopic region. The size of localization reaches to the optical diffraction limit. The localized surface plasmons are also usable as a measurement probe of refractive index as well as the conventional surface plasmons, which propagate in one direction on the metal surface [44]. In addition, the positive characteristics of the conventional surface plasmons are maintained. The localization technique reduces the sensing volume to $< 10$ al for typical setups and samples. The small measurement probe is useful in the detection of influenza viruses with a certain subtype. Since the size of the viruses is $\sim 100$ nm, the measurement method has a potential to detect a single virus. Moreover, it is possible to detect multiple subtypes in one measurement from a sample with an ultra small volume.

## 1.2 Determination of influenza viruses with specific subtypes

Influenza A and B viruses cause the infectious diseases in humans and animals. In fact, influenza A viruses cause a pandemic in the world. Influenza A virus has eight single segments RNA. The surface of the virus is covered by two kinds of glycoproteins. They are hemagglutinin (HA) and neuraminidase(NA). Hemagglutinin is responsible for binding host cell, and neuraminidase is responsible for releasing replicated viruses from infectious cells. Influenza A virus is labeled according to the type of hemagglutinin and neuraminidase it carries. Up to date, 17 types of hemagglutinin and 9 types of neuraminidase is identified. This means that, in theory, there are153 different subtypes of influenza viruses. Each virus has a different degree of virulence and pathogen. Subtype determination of influenza virus, which is equal to determining the types of hemagglutinin and neuraminidase, plays an important role on the front line of research in research institutes of infection desease. A fast and high sensitive determination method is desired, because it helps to speed up research [45–49].

At the present, there are two methods which are frequently used to determine the subtype of influenza virus in the research institute [50–52]. One is based on genetic analysis. In this method, a sample is collected from the nostril, and swab sample is dissolved in Phosphate Buffered Saline (PBS). A target sequence of RNA is then transcribed to a DNA sequence. After DNA molecules are amplified by polymerase chain reaction (PCR), amplified DNA molecules are determined by using electrophoretic separation [53,54]. This method has high sensitivity, but its limitation is difficult to overcome, the process of DNA amplification takes several hours. A fast method for subtype determination is desired.

The other method is based on immuno-flourescence analysis [55, 56]. In this method, monoclonal antibodies as primary antibodies are immobilized on the substrate surface, and they interact with the target viruses which bind on the sensing surface. After that secondary antibodies is given on the substrate surface to interact with viruses and are fixed

on the substrate surface. The secondary antibodies are labeled by fluorescent particles. Fluorescence is detected to determine the subtype of an influenza virus. In this method, labeled antibodies are used in the process of virus detection. If a method do not require secondary antibodies, it is possible to increase the detection speed and remove the post chemical process. A determination method without secondary antibodies is expected, which contributes to a survey of infectious diseases in medical institutes.

This study aimed to develop a method to determine the subtype of influenza virus using antigen/antibody interactions. In this method, a localized surface plasmon as a sensing probe is used to measure the refractive index variation that arises from interactions between influenza viruses and their monoclonal antibodies on the sensing surface. This method has good properties, such as high sensitivity, fast response, free label, and real time monitoring [57–59]. Because it is possible for a localized surface plasmon to produce an ultra small sensing probe, it has the potential to detect a single influenza virus. If multiple kinds of monoclonal antibodies are immobilized in microscopic sections on the sensing surface, parallel determination of the subtype is achievable from a sample with small volume.

## 1.3 Research purpose

The present research dealt with the development of an optical sensor to determine multiple subtypes of influenza viruses from a sample with ultra small volume in the one measurement. In this technique, multiple subtypes of antibodies are immobilized on the sensing surface: they in turn can be used to detect the influenza viruses with multiple subtypes. For this purpose, an ultra small sensing region is required as well as the localization of a surface plasmon to produce a micro/nano size of the sensing region. This localized surface plasmon excited on a flat metal surface in microscopic region is used as a sensing probe to measure the refractive index variation.

This study demonstrates that the sensing method using localized surface plasmons is able to distinguish the subtypes of influenza virus between A/H1N1 and A/H3N2 by using monoclonal antibodies for A/H1N1. To evaluate applicability of the developed sensor to medical diagnosis used in the real word, a nasal swab specimen was detected under the same condition for A/H1N1 detection.

# Chapter 2 Surface plasmon sensing

The propagation constants of surface plasmons are useful for monitoring the refractive index variation on a metal surface. The development of optical biosensors based on surface plasmons has attracted wide attention because of their high sensitivity in measuring the refractive index [60–63]. Surface plasmon as a sensing probe of refractive index measurement is useful for the detection of biomolecular interactions [64–71]. In this chapter, the sensing technique based on surface plasmons is described.

## 2.1 Surface plasmon

Surface plasmon is a quantum of free electron oscillations excited on a metal surface [1,3]. Figure 1 (a) shows free electron distribution on the metal surface. Because of coulomb force, free electrons move from high density to low density area. Due to inertia, density change as shown in Fig. 1 (b), and the above mentioned movement of free electrons is repeated. This repetitive movement brings about a collective oscillation, which is referred to as surface plasmon. Under a particular configuration, if a light with appropriate polarization and incident angle reflects on a metal surface, surface plasmons are excited on the metal surface. The dispersion relation of surface plasmon strongly depends on the refractive index on the metal surface. Surface plasmons can be used as a sensing probe for measuring the refractive index variation on the metal surface.

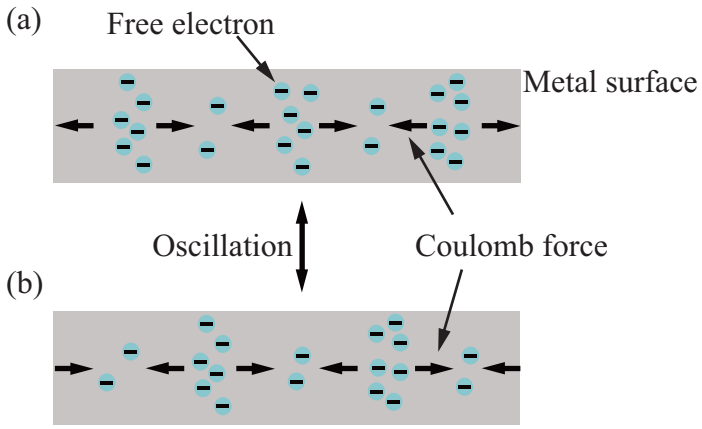


Fig. 1: Collective oscillations of free electrons on the metal surface.

### 2.1.1 Dispersion relation of surface plasmons

The propagating constant $k_{light}$ of light propagating in the medium with refractive index $n$ can be expressed by the equation below [1].

$$k_{light} = \frac{\omega}{c} n. \tag{2.1}$$

In this equation, $\omega$ and $c$ indicate the angular frequency and light speed in vacuum, respectively. The relation between angular frequency and propagating constant is called dispersion relation of light.

In the model as shown in Fig. 2, the dispersion relation of surface plasmons propagating along the interface between metal and dialectic can be derived as follows.

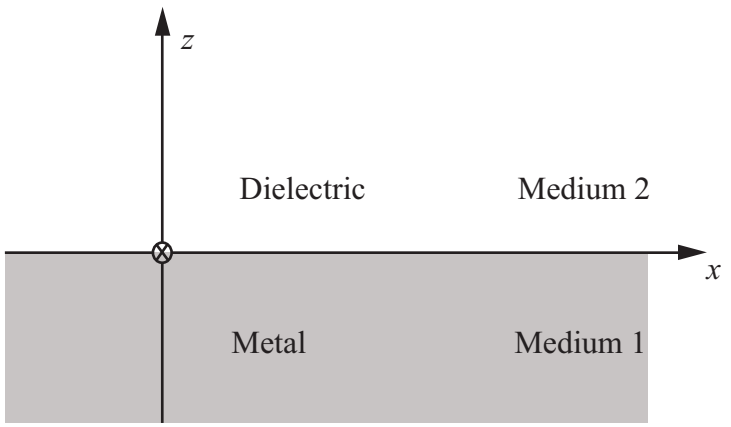


Fig. 2: Model for deriving dispersion relation of surface plasmons .

A surface plasmon is an electromagnetic wave having components of electric field $\boldsymbol{E}$ and magnetic field $\boldsymbol{H}$, which satisfy the Mexwell's equations. Maxwell' equations are expressed by following.

$$\nabla \times \boldsymbol{E} = -\frac{\partial \boldsymbol{B}}{\partial t} \tag{2.2}$$

$$\nabla \times \boldsymbol{H} = \frac{\partial \boldsymbol{D}}{\partial t} \tag{2.3}$$

$$\nabla \cdot \boldsymbol{D} = 0 \tag{2.4}$$

$$\nabla \cdot \boldsymbol{B} = 0 \tag{2.5}$$

In the isotropic medium,

$$\boldsymbol{D} = \varepsilon \boldsymbol{E} \tag{2.6}$$
$$\boldsymbol{B} = \mu \boldsymbol{H} \tag{2.7}$$

in which, $\varepsilon$ and $\mu$ are permittivity and magnetic permeability of medium, respectively. Components of electric $\boldsymbol{E}$ and magnetic $\boldsymbol{H}$ field vectors are as follows.

$$\boldsymbol{E} = (E_x, E_y, E_z) \tag{2.8}$$
$$\boldsymbol{H} = (H_x, H_y, H_z) \tag{2.9}$$

In here,

$$\nabla \times \boldsymbol{H} = \left( \frac{\partial H_z}{\partial y} - \frac{\partial H_y}{\partial z}, \frac{\partial H_x}{\partial z} - \frac{\partial H_z}{\partial x}, \frac{\partial H_y}{\partial x} - \frac{\partial H_x}{\partial y} \right). \tag{2.10}$$

From equation (2.3), (2.6), and (2.10), the following functions are derived by replacing $\dfrac{\partial}{\partial t}$ by $i\omega$.

$$\frac{\partial H_z}{\partial y} - \frac{\partial H_y}{\partial z} = i\omega\varepsilon E_x \tag{2.11}$$
$$-\frac{\partial H_z}{\partial x} + \frac{\partial H_x}{\partial z} = i\omega\varepsilon E_y \tag{2.12}$$
$$\frac{\partial H_y}{\partial x} - \frac{\partial H_x}{\partial y} = i\omega\varepsilon E_z \tag{2.13}$$

In order to reflect the oscillation mode of the surface plasmon, $TM$ wave is assumed here. The electric field and magnetic field are shown in following equations.

$$\boldsymbol{E} = (E_x, 0, E_z) \tag{2.14}$$
$$\boldsymbol{H} = (0, H_y, 0) \tag{2.15}$$

Consequently, the equations below are obtained.

$$-\frac{\partial H_y}{\partial z} = i\omega\varepsilon E_x \tag{2.16}$$
$$\frac{\partial H_y}{\partial x} = i\omega\varepsilon E_z \tag{2.17}$$

Then, dependences of magnetic compotes in the $z$ direction in the medium of metal and dielectric are considered as $H_{1y}$ and $H_{2y}$, respectively.

$$H_{1y} = Ae^{-ik_{1z}\cdot z} \tag{2.18}$$
$$H_{2y} = Be^{-ik_{2z}\cdot z} \tag{2.19}$$

Amplitudes $A$ and $B$ are undetermined coefficients. Equations (2.18), (2.19) are applied in equation (2.16) and the following is obtained.

$$-\frac{\partial H_{1y}}{\partial z} = ik_{1z}\cdot Ae^{-ik_{1z}\cdot z} = i\omega\varepsilon_1 E_{1x} \tag{2.20}$$
$$-\frac{\partial H_{2y}}{\partial z} = ik_{2z}\cdot Be^{-ik_{2z}\cdot z} = i\omega\varepsilon_2 E_{2x} \tag{2.21}$$

From boundary conditions $H_{1y}\Big|_{z=0} = H_{2y}\Big|_{z=0}$ and $E_{1x}\Big|_{z=0} = E_{2x}\Big|_{z=0}$, the following equations are derived.

$$A = B \tag{2.22}$$
$$k_{1z}\frac{A}{\varepsilon_1} = k_{2z}\frac{B}{\varepsilon_2} \tag{2.23}$$

From the two equations mentioned above, equation (2.24) is derived.

$$\begin{pmatrix} 1 & -1 \\ \dfrac{k_{1z}}{\varepsilon_1} & -\dfrac{k_{2z}}{\varepsilon_2} \end{pmatrix} \begin{pmatrix} A \\ B \end{pmatrix} = \begin{pmatrix} 0 \\ 0 \end{pmatrix} \tag{2.24}$$

From equation (2.24),

$$\frac{k_{1z}}{\varepsilon_1} = \frac{k_{2z}}{\varepsilon_2} \tag{2.25}$$

is obtained. Further, $k_{1x}$ and $k_{2x}$ should be equal at the interface.

$$k_{1x} = k_{2x} = k_{sp} \tag{2.26}$$

In this equation, $k_{sp}$ is the wavenumber of surface plasmon. The wavenumber in each medium can be expressed as follows.

$$|\boldsymbol{k}_1|^2 = \left(\frac{\omega}{c}\right)^2 \varepsilon_1 \tag{2.27}$$

$$|\boldsymbol{k}_2|^2 = \left(\frac{\omega}{c}\right)^2 \varepsilon_2 \tag{2.28}$$

From the three equations above,

$$\left(\frac{\omega}{c}\right)^2 \varepsilon_1 = k_{sp}^2 + k_{1z}^2 \tag{2.29}$$

$$\left(\frac{\omega}{c}\right)^2 \varepsilon_2 = k_{sp}^2 + k_{2z}^2 \tag{2.30}$$

are obtained. From equation (2.25),

$$k_{1z} = \frac{\varepsilon_1}{\varepsilon_2} k_{2z}. \tag{2.31}$$

Equation (2.31) is substituted into equation (2.29),

$$k_{sp}^2 + \left(\frac{\varepsilon_1}{\varepsilon_2}\right)^2 k_{2z}^2 = \left(\frac{\omega}{c}\right)^2 \varepsilon_1. \tag{2.32}$$

From equation (2.30), the equation below

$$k_{2z}^2 = \left(\frac{\omega}{c}\right)^2 \varepsilon_2 - k_{sp}^2 \tag{2.33}$$

is obtained. From equation (2.32) and (2.33), $k_{sp}$ can be expressed in the following equation.

$$k_{sp} = \frac{\omega}{c}\sqrt{\frac{\varepsilon_1 \varepsilon_2}{\varepsilon_1 + \varepsilon_2}} \tag{2.34}$$

By expressing, permittivity of metal and sample as $\varepsilon_m(\omega)$ and $\varepsilon_s(\omega)$, equation (2.34) becomes as follows.

$$k_{sp}\left(\omega\right) = \frac{\omega}{c}\sqrt{\frac{\varepsilon_m\left(\omega\right)\varepsilon_s\left(\omega\right)}{\varepsilon_m\left(\omega\right) + \varepsilon_s\left(\omega\right)}} \tag{2.35}$$

By employing plasma frequency $\omega_p$ of the Drude-model, real part of metal permittivity $\varepsilon_{mr}$ can be expressed as follows.

$$\varepsilon_{mr}\left(\omega\right) \simeq 1 - \frac{\omega_p^2}{\omega^2} \tag{2.36}$$

By assuming vacuum for medium on the metal ($\varepsilon_s = 1$ ),

$$\begin{aligned} Real\Big\{k_{sp}(\omega)\Big\} &= \frac{\omega}{c}\sqrt{\frac{\varepsilon_{mr}(\omega)}{\varepsilon_{mr}(\omega)+1}} \\ &\simeq \frac{\omega}{c}\sqrt{\frac{1-\omega_p^2/\omega^2}{2-\omega_p^2/\omega^2}} \\ &= \frac{\omega}{c}\sqrt{\frac{\omega^2-\omega_p^2}{2\omega^2-\omega_p^2}}. \end{aligned} \tag{2.37}$$

This equation can be expressed as follows.

$$Real\Big\{k_{sp}(\omega)/\left(\frac{\omega_p}{c}\right)\Big\} \simeq \frac{\omega}{\omega_p}\sqrt{\frac{\left(\frac{\omega}{\omega_p}\right)^2 - 1}{2\left(\frac{\omega}{\omega_p}\right)^2 - 1}}. \tag{2.38}$$

According to equation (2.38), the plot of propagating constant $k_{sp}$ as a function of angular frequency $\omega$ is shown as in Fig. 3. One can see the that $k_{sp}$ is saturated at $1/\sqrt{2}$ of $\omega/\omega_p$ axis, and plot is tangent to linear line describing maximum spatial frequency of propagating light in the vacuum. As a consequence, the propagating light in vacuum cannot excite the surface plasmons because $k_x$ of light and surface plasmon never coincide.

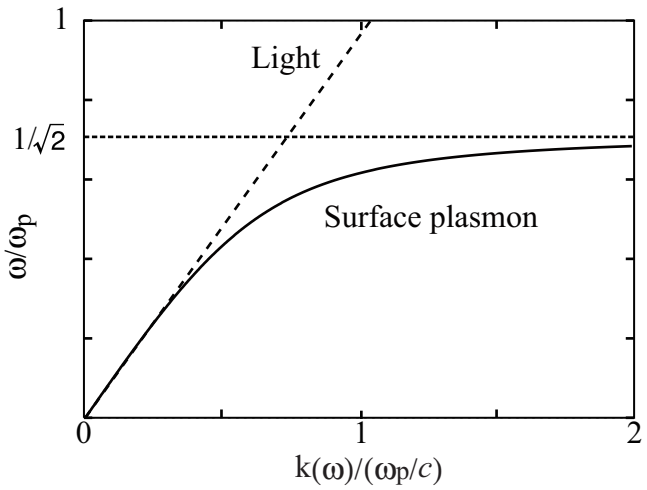


Fig. 3: Dispersion relation of a surface plasmon and light in the vacuum.

### 2.1.2 Excitation of surface plasmons

For the excitation of surface plasmons, a particular optical setup is necessary. Among the setups to excite the surface plasmons, Kretschmann configuration is frequently used for this purpose. The said configuration is shown in the Fig. 4. It consists of a prism as a dielectric medium with high refractive index, and a metal film covered by air as a dielectric medium with low refractive index.

In this method, an illumination light with appropriate polarization is reflected at the interface between the metal film and the prism, in which the incident light is larger then the critical angle. The evanescent wave appears in the metal surface, and its intensity exponentially decreases from the metal surface. Once the incident angle increases, the wavenumber of illumination light increases in medium of prism. The light with excitation angle of surface plasmon can be used to excited the surface plasmons on the metal surface.

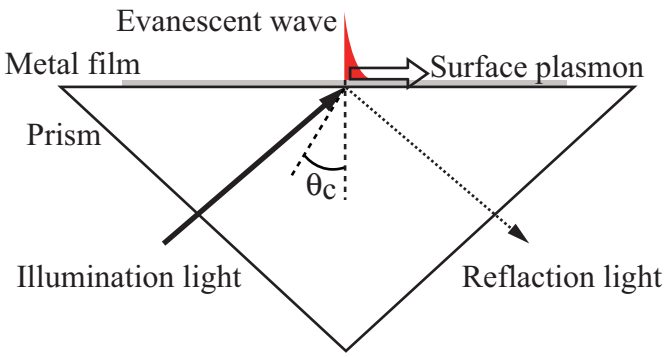


Fig. 4: Kretschmann configuration

### 2.1.3 Other configuration for the excitation of surface plasmons

Except Kretschmann configuration, Otto and Wood configurations, which are used to excite the surface plasmons, are described here. Figure 5 shows the Otto configuration, which consists of a dielectric with high refractive index (glass prism), a metal, and a dielectric with low refractive index. Incident light with appropriate polarization ($p$-polarization) and an incident angle that is larger than the critical angle produces the evanescent wave in the metal surface. The intensity of electric field exponentially decreases, so that a distance between the prism and the metal surface should be within of ∼100 nm. The illumination light with an excitation angle, surface plasmons are excited on the metal surface.

Figure 6 shows a wood configuration, in which light illuminates the grating surface [2, 72]. The non-radiation component of diffracted light excites the surface plasmon on the grating surface.

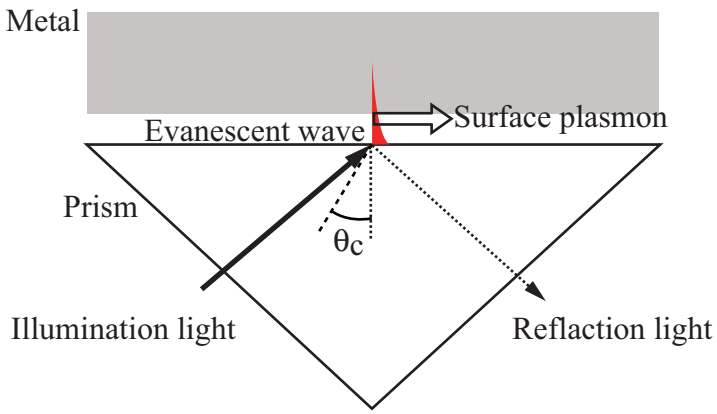


Fig. 5: Otto configuration.

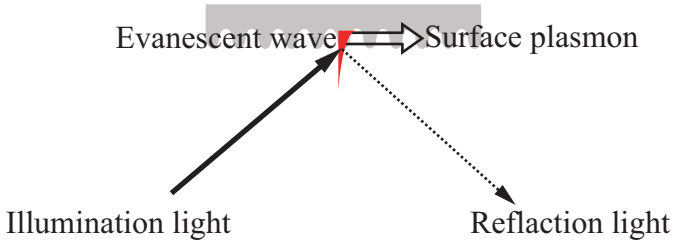


Fig. 6: Wood configuration.

## 2.2 Refractive index measurement by using surface plasmons

### 2.2.1 Calculation theory of reflectivity in Kretschmann configuration

In the Kretschmann configuration, reflectivity as a function of incident angle for illumination light is simulated in this section [73, 74]. Figure 7 shows the calculation model based on Kretschmann configuration, which consists of a dielectric medium with high refractive index $n_1$, gold film with refractive index $n_2$, and a dielectric medium with low refractive index ($n_3$). Regarding illumination light with p-polarization, wavelength $\lambda_0$ in vacuum incident angle $\theta_1$ is assumed.

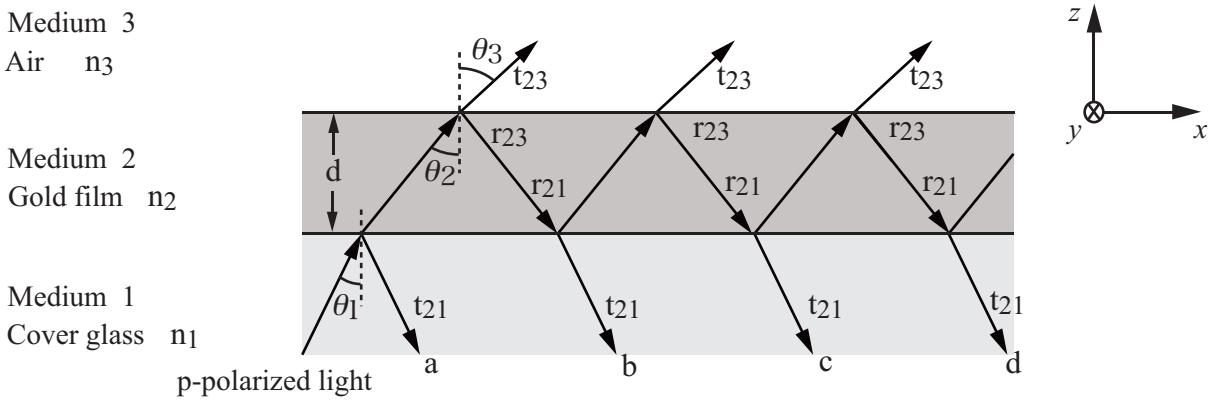


Fig. 7: The calculation model based on Kretschmann configuration.

From the side of a dielectric with high refractive index , light is first reflected at the interface between the dielectric with hight refractive index and the gold film. Reflected light is assumed $a$, $b$, $c$,$\cdots$. The sum of each reflected light is reflectivity $r$ of illumination light in the Kretschmann configuration.

The reflectivity $r_{ij}$ and transmissivity $t_{ij}$ of illumination light at the interface two mediums with refractive index $n_i$ and $n_j$ are expressed by as following equations.

$$r_{ij} = \frac{n_j \cos\theta_i - n_i \cos\theta_j}{n_j \cos\theta_i + n_i \cos\theta_j} \tag{2.39}$$

$$t_{ij} = \frac{2n_i \cos\theta_i}{n_j \cos\theta_i + n_i \cos\theta_j} \tag{2.40}$$

And they have the following relationship.

$$t_{ij}t_{ji} = 1 + r_{ij}r_{ji} \tag{2.41}$$

Using the equations above, each reflected $a$, $b$, $c$,$\cdots$ can be shown as:

$$\begin{aligned}
&a : r_{12} \\
&b : t_{12}e^{ik_{2z}d} \cdot r_{23}e^{ik_{2z}d} \cdot t_{21} \\
&c : t_{12}e^{ik_{2z}d} \cdot r_{23}e^{ik_{2z}d} \cdot t_{21} \cdot r_{21}e^{ik_{2z}d} \cdot r_{23}e^{ik_{2z}d} \cdot t_{21} \\
&\vdots
\end{aligned}$$

Reflectivity $r$ can be presented as the following.

$$\begin{aligned}
r &= a + b + c + \cdots \\
&= a + \alpha + \alpha\beta + \cdots \\
&= a + \alpha(1 + \beta + \beta^2 + \beta^3 + \cdots) \\
&= a + \frac{\alpha}{1-\beta} \\
&= r_{12} + \frac{t_{12}t_{21}r_{23}e^{i2k_{2z}d}t_{21}}{1 - r_{21}r_{23}e^{i2k_{2z}d}}
\end{aligned}$$

In which, depending on equation (2.41),

$$\begin{aligned}
r &= r_{12} + \frac{(1 + r_{12}r_{21})r_{23}e^{i2k_{2z}d}}{1 - r_{21}r_{23}e^{i2k_{2z}d}} \\
&= \frac{r_{12} + r_{23}e^{i2k_{2z}d}}{1 - r_{21}r_{23}e^{i2k_{2z}d}}
\end{aligned} \tag{2.42}$$

the above equation is obtained. Intensity of reflectivity $R$ is expressd in the next equation.

$$R = |r|^2 = r \cdot r^* \tag{2.43}$$

Equations (2.42) and (2.43) are used to calculate the reflactance of reflected light.

### 2.2.2 Relationship between incident angle and reflectivity

The calculated results of reflectivity in the Kretschmann configuration are shown in Fig. 8. In this calculation, it is assumed that the Kretschmann configuration consists of a glass with refractive index of 1.515 and gold film with refractive index of $0.2038+i3.318$ and an air with refractive index of 1.000. The wavelength of illumination light is 632.8 nm.

One can see that the plot dips at the 44.04° in Fig. 8 (a); this is because excited surface plasmons absorbed the energy of illumination light. The absorption angle is referred to as the excitation angle of surface plasmon. This angle is strongly depends on the refractive index of the medium which coveres on the metal surface. Based on these properties, it is possible to measured the refractive index of a medium on the metal surface by using the monitored absorption angle. Reflectivity for s-polarization can be calculated by using Fresnel coeeficient for s-polarization. As shown in Fig. 8 (b), there are no absorption dip for s-polarization because s-polarization can not couple to TM mode oscillation.

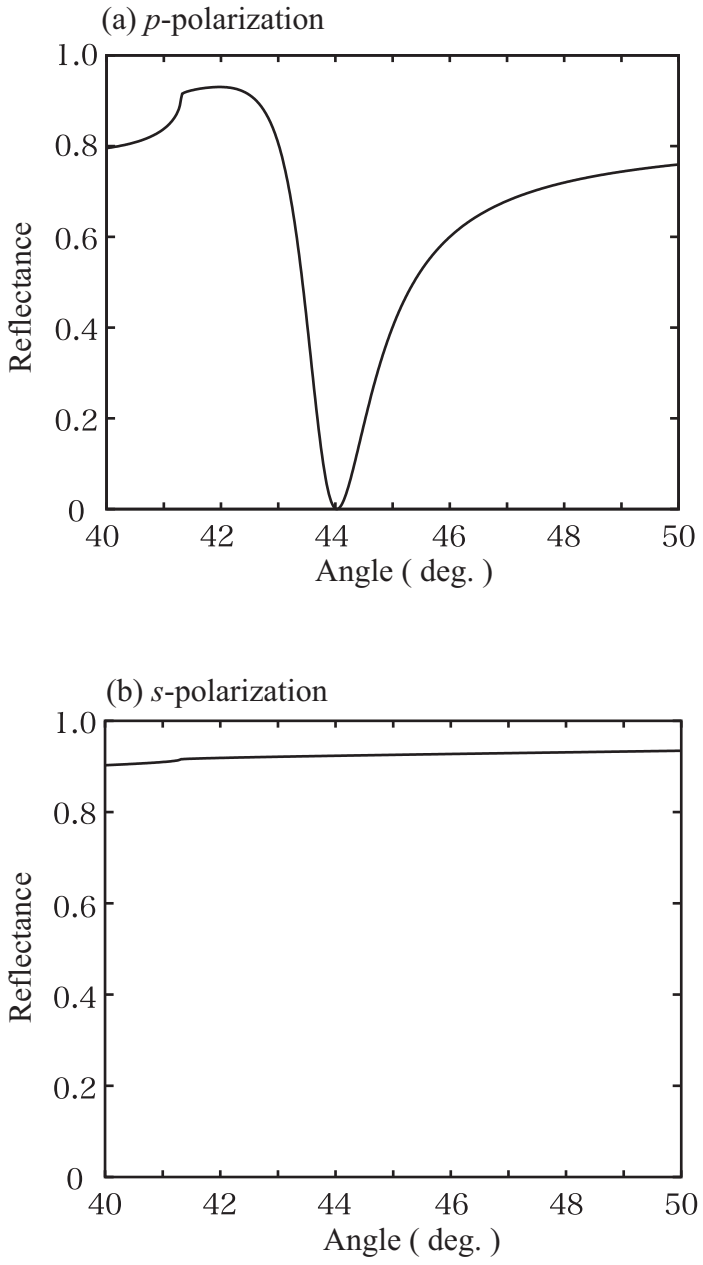


Fig. 8: Reflectance as a function of incident angle for p- and s-polarization.

### 2.2.3 Relationship between thickness of metal film and reflectivity

The thickness of metal films affects the efficiency of energy transfer from excitation light to surface plasmons. In this subsection, the relationship between thickness of metal film and reflectivity is shown. Figure 9 shows the calculation results of reflectivity under different thickness of gold films. In this calculation, it is assumed that Kretschmann configuration consists of glass with refractive index of 1.515 and gold film with refractive index of $0.2038+i3.318$ and air with refractive index of 1.000. The metal thickness is 27.47, 47.47, and 67.47 nm, respectively. The wavelength of illumination light is 632.8 nm. Based on these calculation shown in the Fig. 9, one can see that there are the different excitation angles and that reflectivity depending on the thickness of metal film. If the thickness is thinner than 47.47 nm, its excitation angle, the full width at the half minimum, and reflectivity increase in the comparison between that of 47.47nm. If the thickness is thicker than 47.47 nm, its excitation angle and the full width at the half minimum remain almost the same, and reflectivity increases. Suitable thickness of metal film for Kretschmann configuration is decided by its lowest reflectivity.

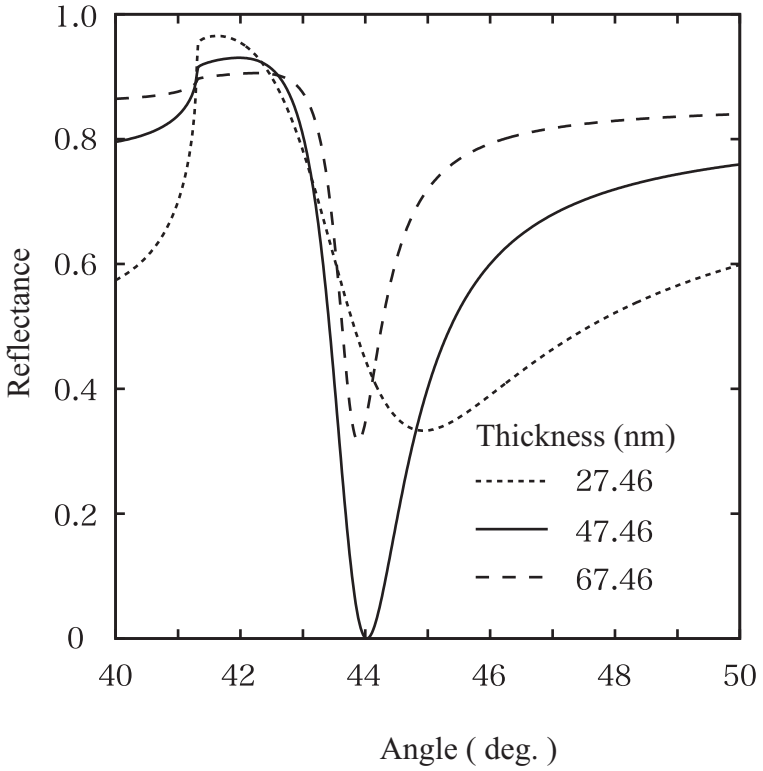


Fig. 9: Reflectance as a function of thickness of metal film.

### 2.2.4 Relationship between refractive index of metal film and reflectivity

The type of metal film affects the full width at half minimum in the Kretschmann configuration. Figure 10 shows the plots of reflectivity versus the incident angle for silver and gold film. In this calculation, it is assumed that Kretschmann configuration consists of glass with refractive index of 1.515, silver film with refractive index $0.0666+i4.045$, gold film with refractive index of $0.2038+i3.318$ and air with refractive index of 1.000. Thickness of silver and gold film are 54.43 and 47.46 nm. It can be seen that they have different excitation angle 42.98 and 44.04°. The full width at half minimum for silver is smaller than the gold. So that, the measurement sensitivity of the refractive index for silver is higher than gold. Although gold film provides lower sensitivity it can bind with the thiol group of biomolecules, so has advantage in preparing the substrate which is covered by recognizing molecules for target bio-molecules.

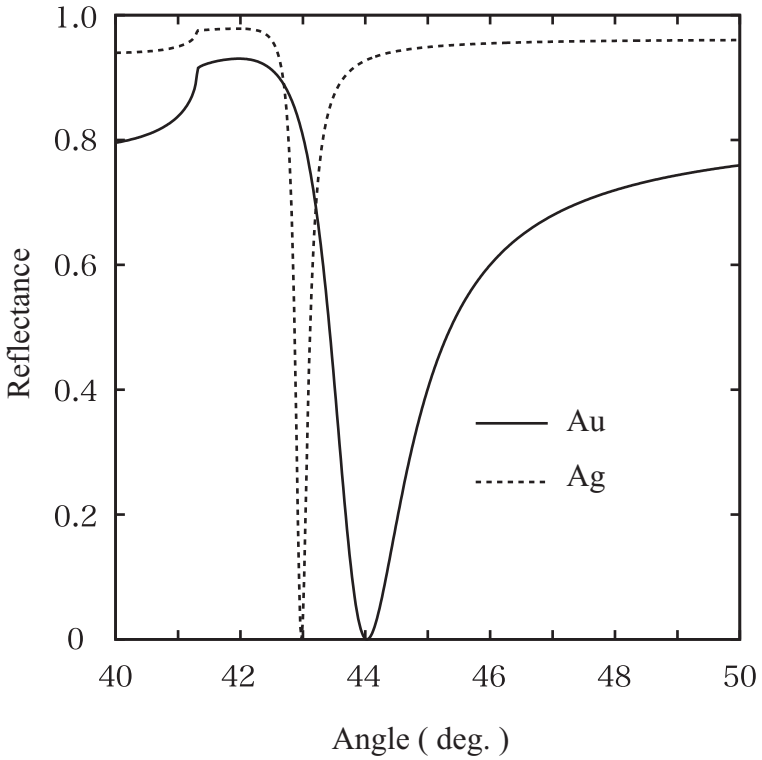


Fig. 10: Reflectance as a function of the silver and the gold film.

### 2.2.5 Measurement principle of refractive index

It is assumed that Kretschmann configuration consists of glass, metal, and sample with refractive indices of $n_g$, $n_m$, and $n_s$, respectively. The propagating constant $k_{sp}$ can be approximately expressed by the equation below.

$$k_{sp} \cong \frac{\omega}{c}\left(\frac{n_m^2 n_s^2}{n_m^2 + n_s^2}\right)^{\frac{1}{2}}$$

When surface plasmons are excited on the metal surface, spatial frequency of of the light on the metal surface should equal to the propagating constant of metal. So that, incident angle $\theta_{sp}$ can be expressed by the equation below.

$$\theta_{sp} = \sin^{-1}\frac{Real\{k_{sp}\}}{n_g\frac{\omega}{c}} \cong \sin^{-1}\left\{\frac{1}{n_g}Real\left\{\left(\frac{n_m^2 n_s^2}{n_m^2 + n_s^2}\right)^{\frac{1}{2}}\right\}\right\}$$

Therefore, by using this equation, the refractive index on the metal can be measured through the excitation angle of the surface plasmon.

To see the detail of this measurement, a medium with slightly higher refractive index (1.002) is also assumed on the metal as a sample. Other parameters are the same with the above calculations. Result is shown in Fig.11. Shift of absorption angle is $\sim 0.11°$. Form the shift of excitation angle, the variation of reflective index can be monitored [73–75].

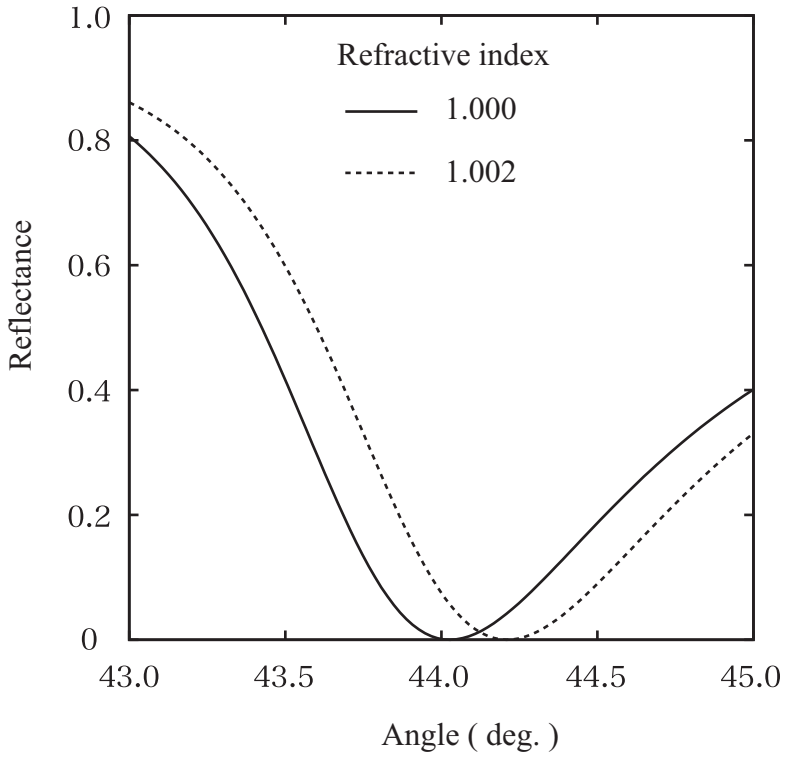


Fig. 11: Reflectance versus angle for different dielectric mediums covering the metal surface.

### 2.2.6 Optical setup of a surface plasmon sensor

In this subsection, two kinds of surface plasmon sensor based on prism coupling are introduced. Figure 12 shows an optical setup of a surface plasmon sensor, which consists of prism, metal film, and array detector. The illumination light is converged on the metal surface through the prism and the reflected light is detected by the array detector. Detector element showing reflection minimum is found to measure the refractive index of a sample on the metal surface.

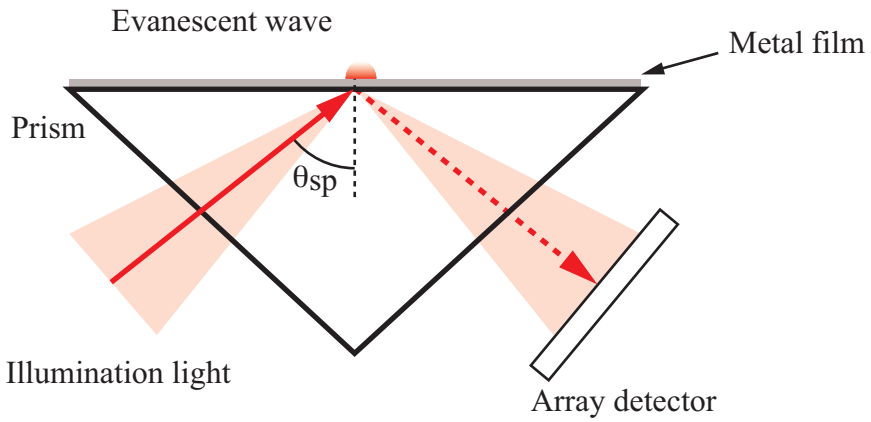


Fig. 12: Angular model of a surface plasmon sensor.

Figure 13 shows the other optical setup as known as the intensity model of a surface plasmon sensor. It consists of prism, and metal film and photodetector. Light beat is reflected on the metal surface through the prism and the reflected light is detected by the photodetector. In this setup, incident angle of illumination light is fixed at a certain angle near the excitation angle of surface plasmon. Intensity of reflected light at the fixed angle is monitored to find variation of the refractive index on the metal.

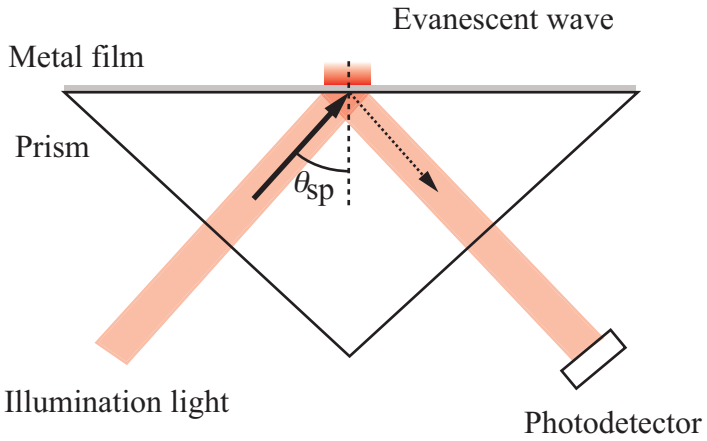


Fig. 13: Intensity model of a surface plasmon sensor.

# Chapter 3 Localized surface plasmon sensor

## 3.1 Localized surface plasmon

Surface plasmon sensor is widely used in detecting molecular binding, because it has high sensitivity and fast response to monitoring the refractive index variation that arise from the interacting ligand and the target molecules. In the conventional surface plasmon sensor based on prism coupling as shown in Fig. 14, excited surface plasmons propagate along the metal surface. In typical cases, the propagating length of the surface plasmon is about several tens of micrometers (about $\sim$10 to 30 $\mu$m ). Due to the propagation of the surface plasmons, reducing the sensing region to a diffracted limit is impossible without decreasing the sensitivity of the conventional surface plasmon sensor based on prism coupling.

With regard to the development of this sensor, decreasing the sensing region to an optical diffraction limit is one of the biggest concerns. Ultra small sensing volume can decrease the requirement for a quantity of biomolecules as a target. With the reduction of sensing volume, it is possible to detect biomolecular interactions from a sample with tiny volume in one measurement.

In this chapter, a method to localize the surface plasmons excited on a flat metal surface in an optical diffraction limit is demonstrated [76–78]. Technique for measuring the change of refractive index by using ocalized surface plasmons and its basic optical setup are introduced.

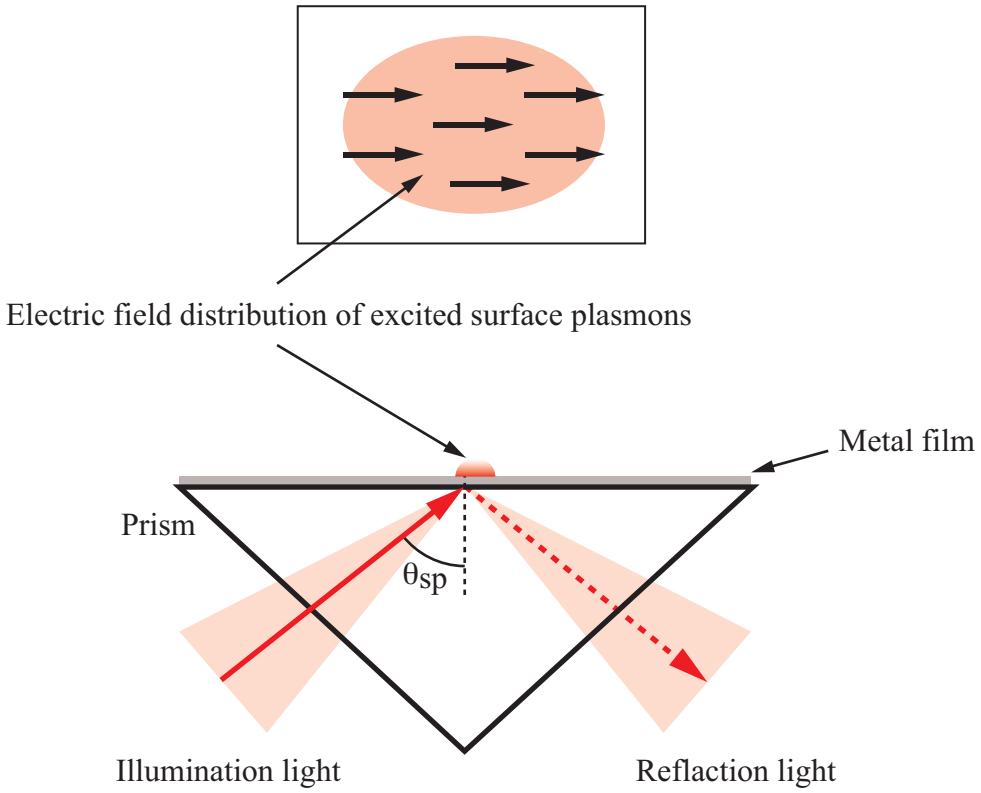


Fig. 14: A conventional setup for the excitation of surface plasmons on a flat metal surface, and its top view in which propagation of surface plasmons is illustrated.

### 3.1.1 Excitation of localized surface plasmons

A surface plasmon sensor for measurements of refractive index on sensing surfaces are recognized as useful tool to monitor bio-molecular interactions among proteins, DNA and some other bio-related molecule. In development of this sensor, reducing the size of sensing region without decreasing the sensitivity to an order of submicrometer is very difficult. A method using localization of excited surface plasmons make it possible to obtain an ultra small sensing region on a flat metal surface. In this subsection, the excitation of localized surface plasmon is demonstrated.

Figure 15 (a) shows the optical setup for the excitation of a localized surface plasmon, which is based on Kretschmenn configuration. It consists of an oil immersion objective lens with a high numerical aperture, a cover glass with a high refractive index and a metal film. Illumination light is focused on the metal surface by using the oil immersion objective lens. Surface plasmons are coherently excited on the metal surface and localized in the diffracted limit region because of their interference with one another. Figure 15 (b) shows the electric field distribution on the flat metal surface; the excited surface plasmons had gathered an ultra small size ($\sim$200 nm).

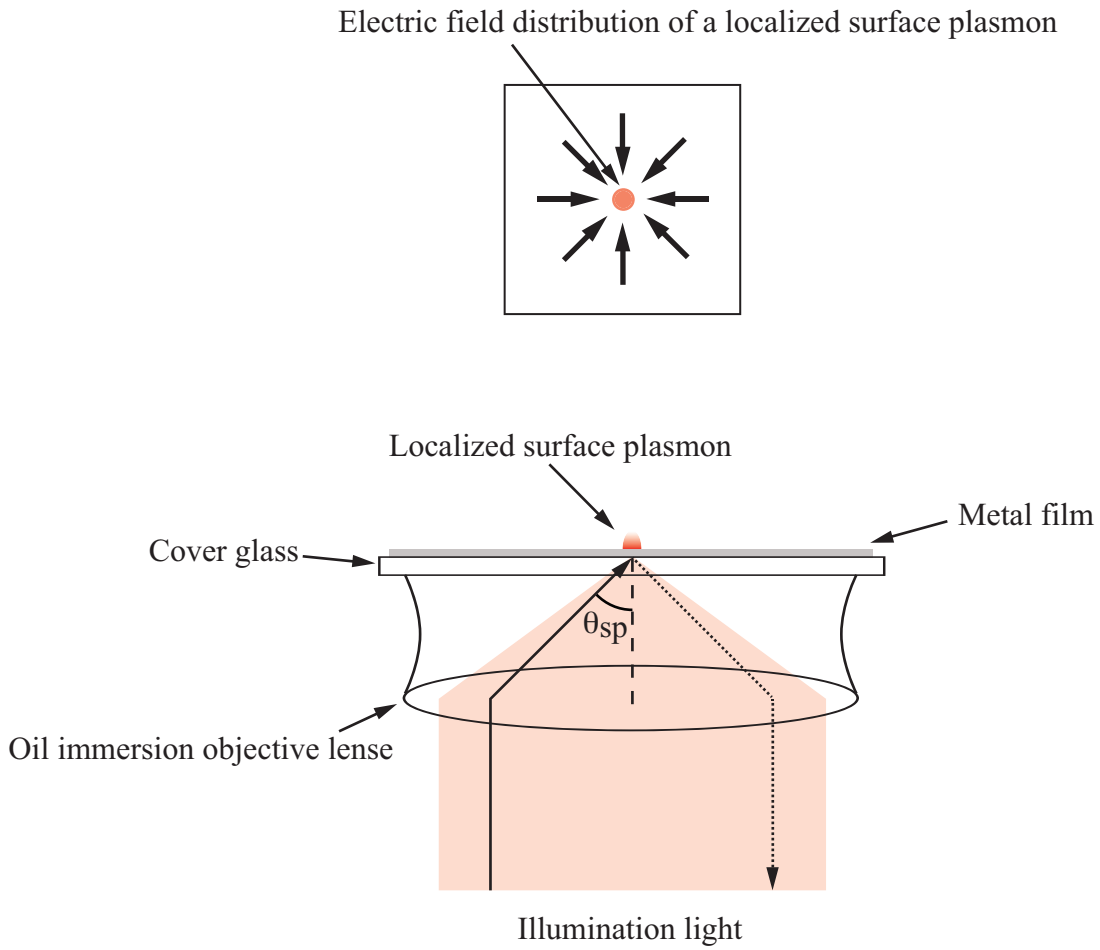


Fig. 15: A setup for the localization of a surface plasmon excited in the microscopic region on the flat metal surface, and its top view in which electric field distribution of a localized surface plasmon is illustrated.

### 3.1.2 The calculation model of electric field distribution on a localized surface plasmons

The focusing light illuminates the Kretschmennn configuration to excited the surface plasmons by using an oil immersion objective lens, and which localize in the microscopic regions [78]. To simulate the electric field distribution of a localized surface plasmon, plane wave components of illumination light involved in the focusing light is traced, the plane wave components superpose under the consideration of multiple reflection in Kretschmennn configuration. Figure 16 shows the calculation model of electric field distribution of localized surface plasmon. As shown in Fig. 16, plane wave components are involved in the focusing light. Figure 16 shows the multiple reflection in Kretschmennn configuration.

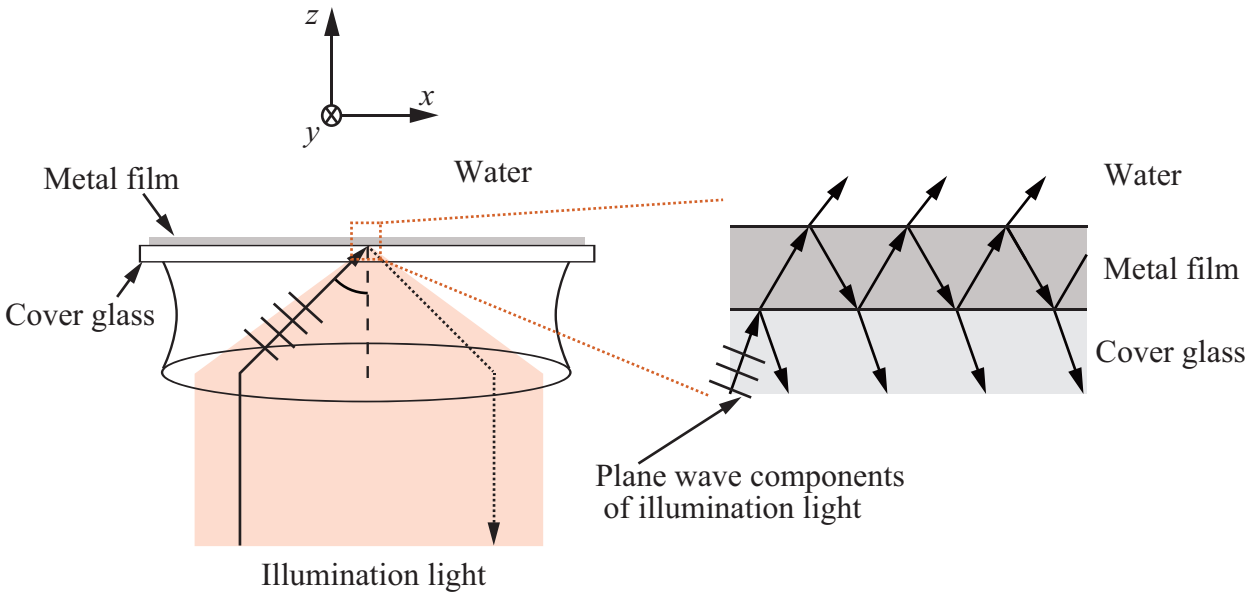


Fig. 16: The plane wave components of illumination light are involved in the focusing light, and right view in which multiple reflection of illumination light in Kretschmennn configuration is illustrated.

Figure 17 shows an assumption which an electric field component $E$ entered the oil immersion objective lens. the light with linear polarization paralleled with $y$ axis illuminates the entrance plane $O-p$, which is divided as $E_r$ and $E_\theta$.

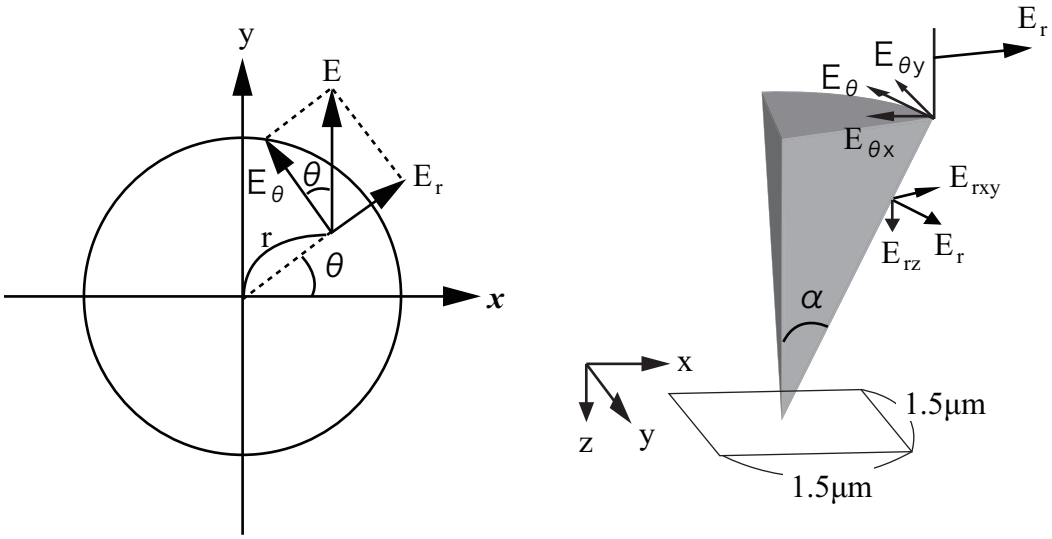


Fig. 17: (a) $y$ component of electric field is divided as $r$, and $\theta$ one. (b) Electric field $E_r$ and $E_\theta$ are expanded as $x$, $y$, $z$ ones.

$$E_r = E\sin\theta \tag{3.1}$$
$$E_\theta = E\cos\theta \tag{3.2}$$

For the derivation of $x$, $y$, $z$ components, $E_r$ passed the entrance pupil plane and tended an angle of $\alpha$ from the optical axis at the focusing point area assumed, As shown in Fig. 17. All of the components of $E_r$ are expressed as follows.

$$E_{rxy} = E_r\cos\alpha \tag{3.3}$$
$$E_{rz} = E_r\sin\alpha \tag{3.4}$$
$$E_{rx} = E_{rxy}\cos\theta \tag{3.5}$$
$$E_{ry} = E_{rxy}\sin\theta \tag{3.6}$$

For the $E_\theta$ component, which just has $x$ and $y$ component, they are shown as equation of (3.7),(3.8).

$$E_{\theta x} = -E_\theta \sin\theta \tag{3.7}$$
$$E_{\theta y} = E_\theta \cos\theta \tag{3.8}$$

In the equations above, $E_x$, $E_y$, $E_z$ components are expressed in equations (3.9),(3.10),(3.11).

$$E_x = E_{rx} + E_{\theta x} \tag{3.9}$$
$$E_y = E_{ry} + E_{\theta y} \tag{3.10}$$
$$E_z = E_{rz} \tag{3.11}$$

According to equations (3.9),(3.10), and (3.11), equation (3.1)∼(3.8) are substituted into equations (3.12),(3.13), and (3.14).

$$E_x = E\sin\theta\cos\theta\left(\cos\alpha - 1\right) \tag{3.12}$$
$$E_y = E\left(\sin^2\theta\cos\alpha + \cos^2\theta\right) \tag{3.13}$$
$$E_z = E\sin\theta\sin\alpha \tag{3.14}$$

In which, equations (3.12),(3.13), and (3.14) are amplitudes of electric field. A item of phase $e^{-i(k_x x + k_y y + k_z z)}$ should be included, so the components of electric field become the following.

$$E_x = E\sin\theta\cos\theta\left(\cos\alpha - 1\right)\cdot\exp\left\{-i\left(k_x x + k_y y + k_z z\right)\right\} \tag{3.15}$$
$$E_y = E\left(\sin^2\theta\cos\alpha + \cos^2\theta\right)\cdot\exp\left\{-i\left(k_x x + k_y y + k_z z\right)\right\} \tag{3.16}$$
$$E_z = E\sin\theta\sin\alpha\cdot\exp\left\{-i\left(k_x x + k_y y + k_z z\right)\right\} \tag{3.17}$$

And then,

$$I_t = |E_x|^2 + |E_y|^2 + |E_z|^2 \tag{3.18}$$

the intensity of electric field is shown in (3.18) equation.

### 3.1.3 Sensing probe regarding the polarization of illumination light

For the evaluation of sensing probe regarding the polarization of illumination light, the distribution of electric field of localized surface plasmons was calculated by the above mentioned model. Figure 18 shows the setup for excitation of a localized surface plasmon illuminated by linear (a) and radial polarized lights (b). A wavelength of illumination light and numerical aperture of objective lens are assumed 632.8 nm and 1.65. The refractive indices of mediums are assumed the real measurement condition and are shown in Table 1.

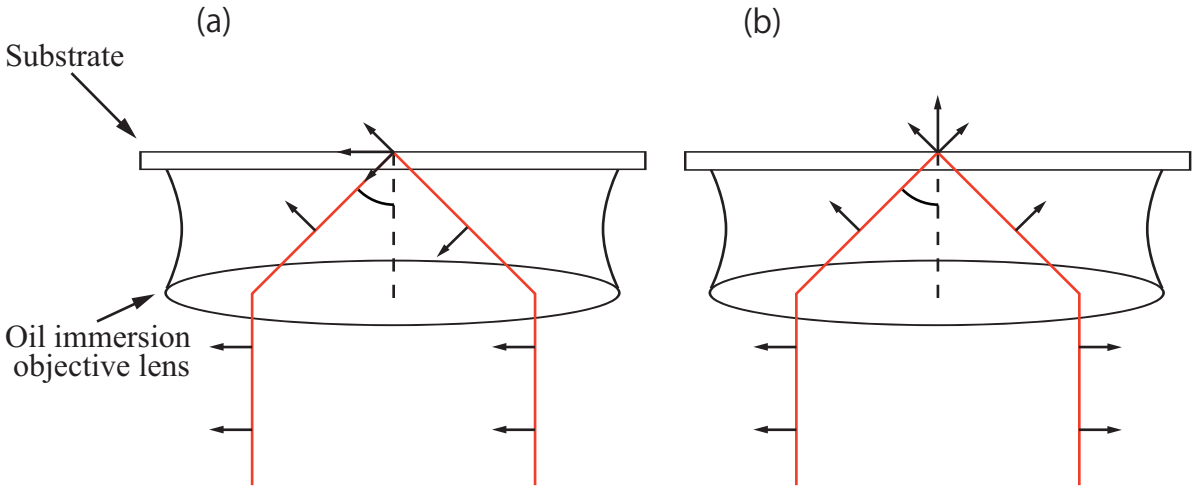


Fig. 18: (a) A conventional setup for the excitation of surface plasmons on the flat metal surface. (b) Electric field distribution of a localized surface plasmon.

Table 1: Used refractive indices of mediums in calculation of electric field distribution

| Medium | Refractive index |
|---|---|
| Cover glass | 1.78 |
| Gold film | 0.2038 + 3.318i |
| Pure water | 1.330 |

If an illumination light has linear polarization, $E_z$ components of electric field distribution is shown in Fig. 19 (a) (pixel number 128 × 128, Size of image 500nm × 500nm), One can see the two spots. In case of a radial polarization like that shown in Fig. 19 (b)(pixel number 128 × 128, Size of image 500nm × 500nm), there is one spot. If a light with radial polarization illumined the setup, the sensing volume is smaller than the one with linear polarization. This increases the resolution of refractive index measurement compared with the linear polarization. So the light with radial polarization is utilized in the real measurement.

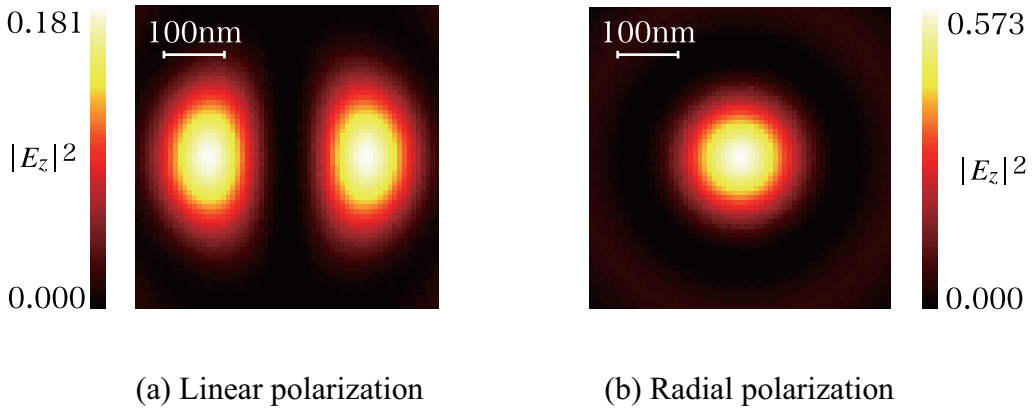


Fig. 19: $E_z$ components of electric field distribution under the illumination light with linear (a) and radial (b) polarization.

### 3.1.4 Sensing volume of a localized surface plasmon sensor

To evaluate the sensing volume of real experiential setup of a localized surface plasmon sensor, the electric field distribution produced by localized surface plasmons was calculated by superposing plane wave components involved in the focusing beam under consideration of multiple reflection in the Kretschmann configuration. In order to simulate the setup, an illumination light with the wavelength of 632.8 nm is assumed, while radial polarization is given at the entrance pupil of the objective lens. The numerical aperture of the objective lens is 1.65. For the substrate, a gold thin film with a refractive index of $0.2038+i3.318$ and a thickness of 44 nm on a cover glass with a refractive index of 1.780 is assumed [79, 80]. Pure water with a refractive index of 1.330 is assumed to cover the substrate surface. Figure 20 (a) and (b) show the simulated intensity distributions of an electric field oscillating in $z$ direction on $xy$ and $xz$ planes. The plots along the dot lines of Fig. 20 (a) and (b) are shown in (c) and (d), as well. For the distribution shown in Fig. 20 (c), the distance from the peak to the first minimum is $\sim$ 180 nm. For that of Fig. 20 (d), the distance with which the electric field intensity decays by a factor of $1/e^2$ is $\sim$ 170 nm.

When it is assumed that the shape of the measurement probe is a cone having the base with a radius of 180 nm and a height of 170 nm, the volume can be calculated as $\sim$ 6 al. As shown in Fig. 21, this measurement probe is fully occupied by seven influenza viruses, which have a diameter of $\sim$ 100 nm.

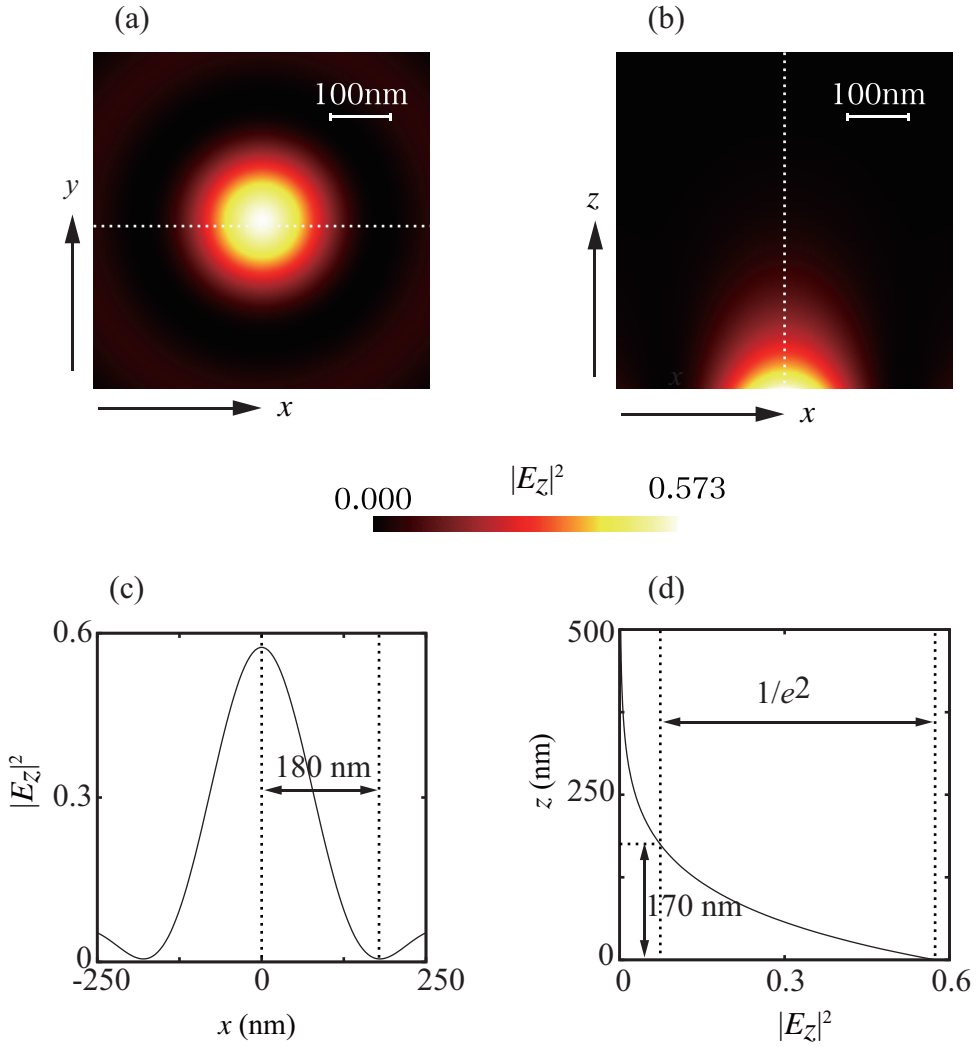


Fig. 20: Intensity distributions of electric fields produced by localized surface plasmons on (a) xy and (b) xz planes, respectively. The plots (c) and (d) represent intensity variations along the dotted lines on the images (a) and (b).

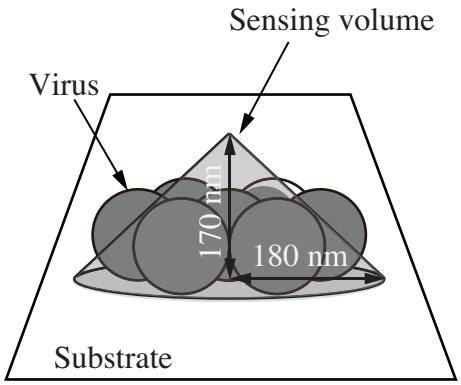


Fig. 21: Sensing probe can be assumed as a cone according to the calculation result of electric field distribution, and it is illustrated with influenza viruses. The cone can be occupied by seven influenza viruses.

## 3.2 Measurement method of refractive index employing a localized surface plasmon

### 3.2.1 Measurement principle

In this subsection, the measurement principle of refractive index by using localized surface plasmon is presented. Figure 22 shows the setup for refractive index measurement using the localized surface plasmon and a typical spatial frequency spectrum at the exit pupil plane recorded by a CCD. The radius of the dark ring $\rho_{sp}$ represents the propagating constant of excited surface plasmons, which strongly depends on effective refractive index on the metal surface. The radius $\rho_{sp}$ can be approximately expressed as follows:

$$\rho_{sp} \cong \mathrm{Real}\left\{\frac{\omega}{c}\left(\frac{n_m^2 n_s^2}{n_m^2 + n_s^2}\right)^{\frac{1}{2}}\right\}. \tag{3.19}$$

In the equation, $\omega$, $c$, $n_m$, and $n_s$ denote angular frequency, light speed in vacuum, complex refractive index of metal film, and effective refractive index on the metal surface, respectively. Variation of the effective refractive index on the metal surface is monitored by analyzing recorded CCD images [81, 82].

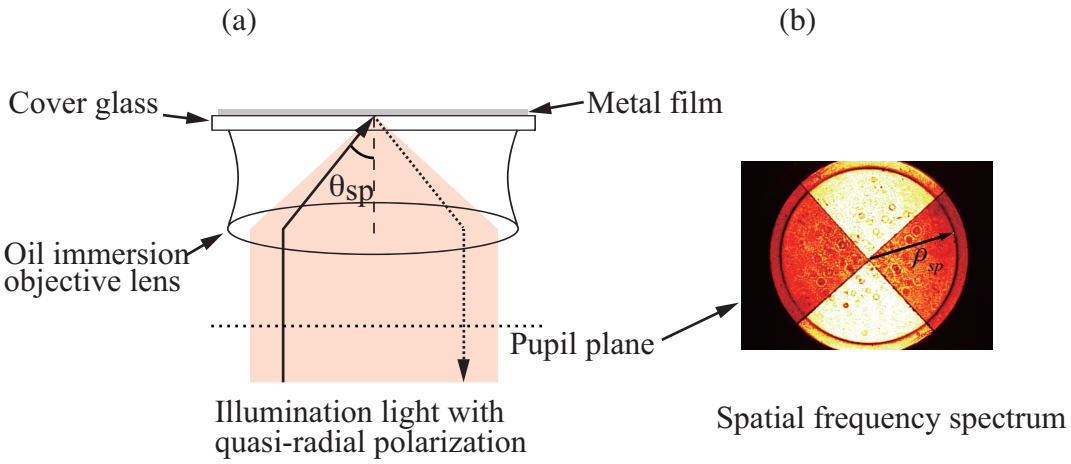


Fig. 22: (a) Optical setup for refractive index measurement by using a localized surface plasmon and (b) spatial frequency spectrum at the exit pupil of an oil immersion objective lens.

### 3.2.2 Optical setup of a localized surface plasmon sensor

Figure 23 shows the basic optical setup of a localized surface plasmon sensor. An He-Ne laser is used as a light source. The expanded laser beam with linear polarization is focused on a gold film by an oil immersion objective lens. The reflected beam is collected by the same objective lens. To obtain spatial frequency distribution of the reflected beam, the intensity distribution at the exit pupil of the objective lens is imaged onto a CCD device. The image recorded by the CCD is transferred to a PC, and is processed to measure the local effective refractive index on the metal surface.

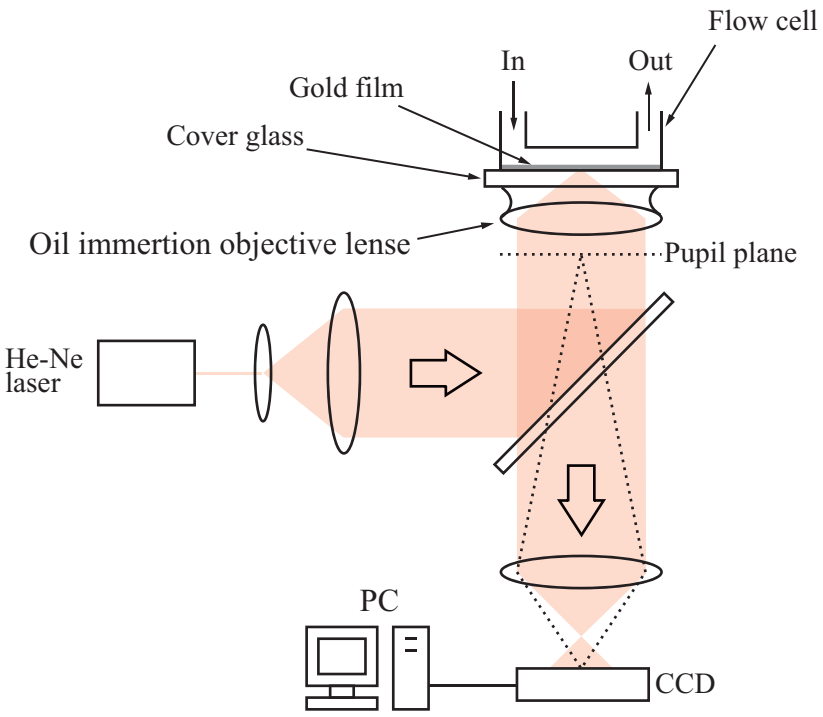


Fig. 23: A basic optical setup of a localized surface plasmon sensor.

# Chapter 4 The measurement stability

In the experiment for virus detection using the conventional surface plasmon sensor from the previous researches [83–87], several liquids were injected into the flow cell. The refractive index variation was monitored in real time. In the experiment, detection time was typically $\sim$ 60 min., the sensitivity was $\sim 10^{-4}$, and high stability after liquid injection was required. At the initial stage of the study, stability by using a prototype of the localized surface plasmon sensor was checked.

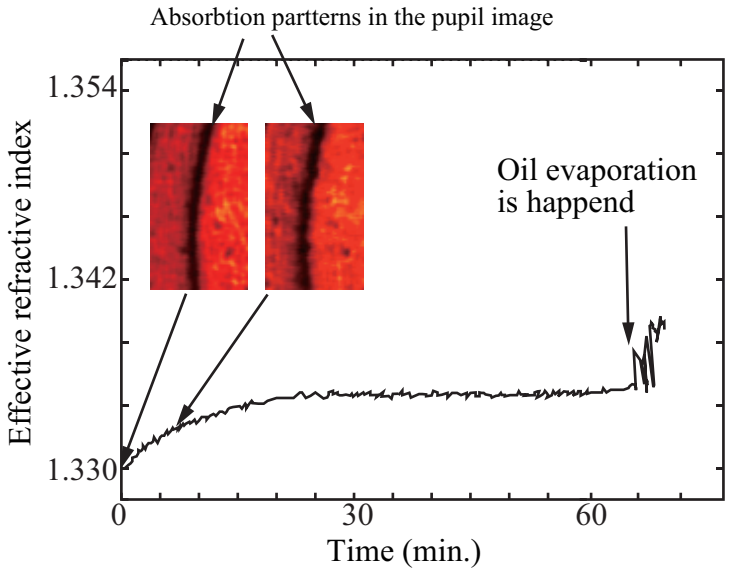


Fig. 24: Illustrated plot of refractive index variation using a prototype localized surface plasmon sensor. Absorption patterns at pupil plane image in different time are inserted inside.

Figure 24 illustrates a typical variation of the refractive index after one shot injection of pure water. The illustration shows that the refractive index gradually increases in the initial $\sim$20 min., and then becomes stable. Stable variation is required after liquid injection in process of virus detection. Because of oil evaporation, detection time should be limited in one hour. This means the available time for virus detection is just 40 min., and this cannot meet the requirements. After checking the pupil plane image, it was found that the absorption pattern is blurred from the initial one. It was caused by stage drift. Detailed analysis is described in the part of this chapter.

Figure 25 illustrates a typical variation of the refractive index after several times of injecting pure water. The illustration shows that the refractive index gradually increases

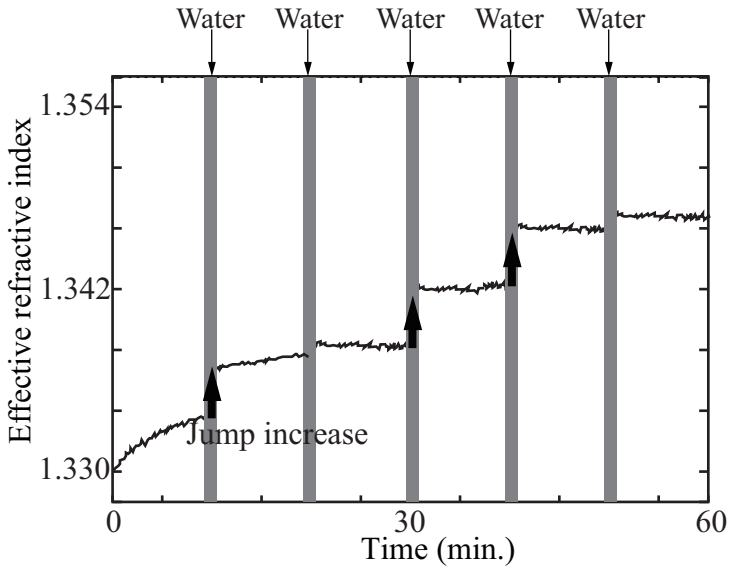


Fig. 25: Illustrated plot of refractive index variation using a prototype localized surface plasmon sensor after several times of liquid injection.

after the initial injection of pure water, which did not happen from the second time injection. Some times after liquid injection, jump increases in refractive index appear in the plot. How to resolve this problem is described in the this chapter.

## 4.1 Correction method of substrate drift

To evaluate the relationship between the problem of substrate drift and refractive index variation, the pupil plane image was checked. Figure 26 (a) shows the substrate located at focusing plane. The pupil image is illustrated in Fig. 26 (c). Figure 26 (b) shows the case in which the substrate is located lower than its original position. The pupil plane image is illustrated in the Fig. 26 (d). One can see that the absorption pattern in Fig. 26 (d) is wider and bigger than the one in Fig. 26 (c). The measured refractive index in the case of substrate movement as shown in Fig. 26 (b) is lagger than the original one. This condition causes the increase in refractive index, as shown in Fig. 27. This happens in most case of measurement after pure water injunction. In contrast, a decrease in refractive index rarely appeared in my experiment.

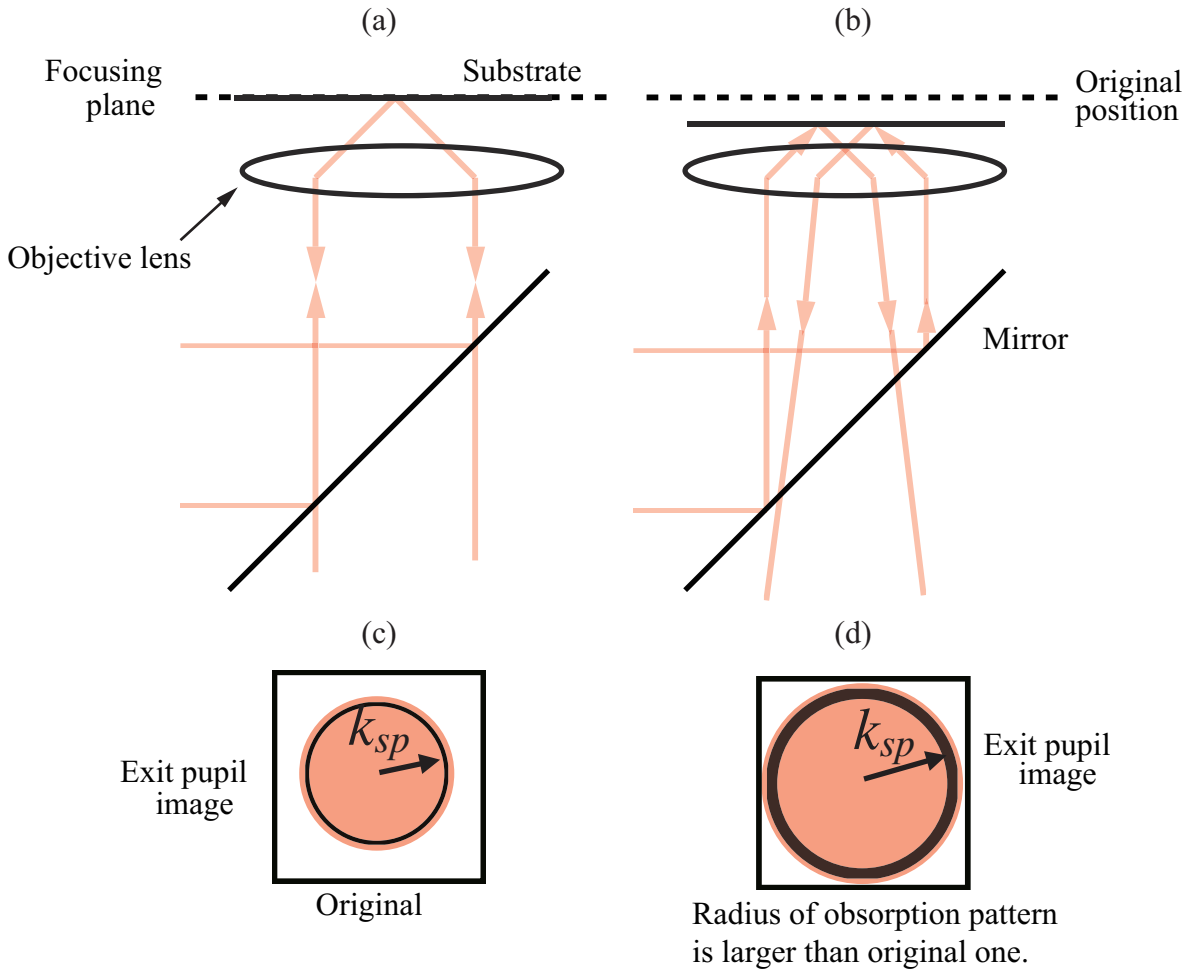


Fig. 26: (a) Substrate located in the focusing plane. (b) Substrate located lower than its original position. (c) and (d) are illustrated pupil plane images under the (a) and (b) situations.

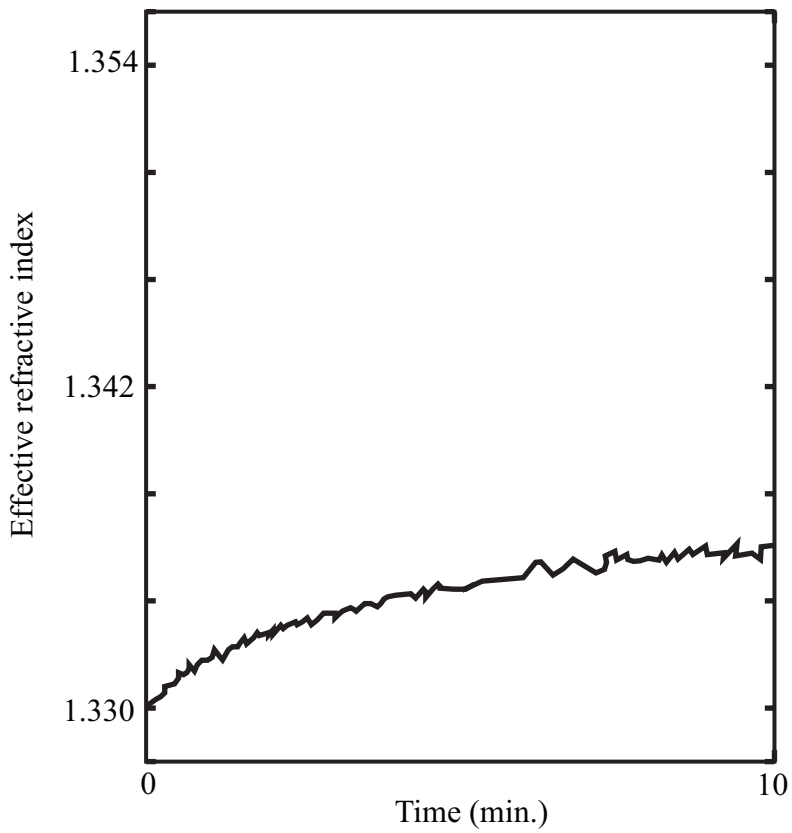


Fig. 27: Illustrated refractive index variation in the initial 10 minutes using a prototype of a localized surface plasmon sensor.

In order to remove the negative influence of the substrate drift, a confocal method was used to correct the position of the substrate during the measurement after liquid injection. Figure 28 shows the correction principle of a substrate drift using a confocal optical system. In this method, reflected light is focused on a point. A detector is placed at the focusing point, as in Fig. 28 (a), and connected with an voltage meter to monitor the intensity of focusing light. If a substrate drifts from the original position, as in Fig. 28 (b) and (c), reflected light is converged or diverged, and then the intensity of reflected light as the focusing point decreases. An illustration of intensity as a function of position of a substrate is shown in the Fig. 29. According to the measured intensity of reflected light, a single is manually given to piezo stage for the correction of a substrate position.

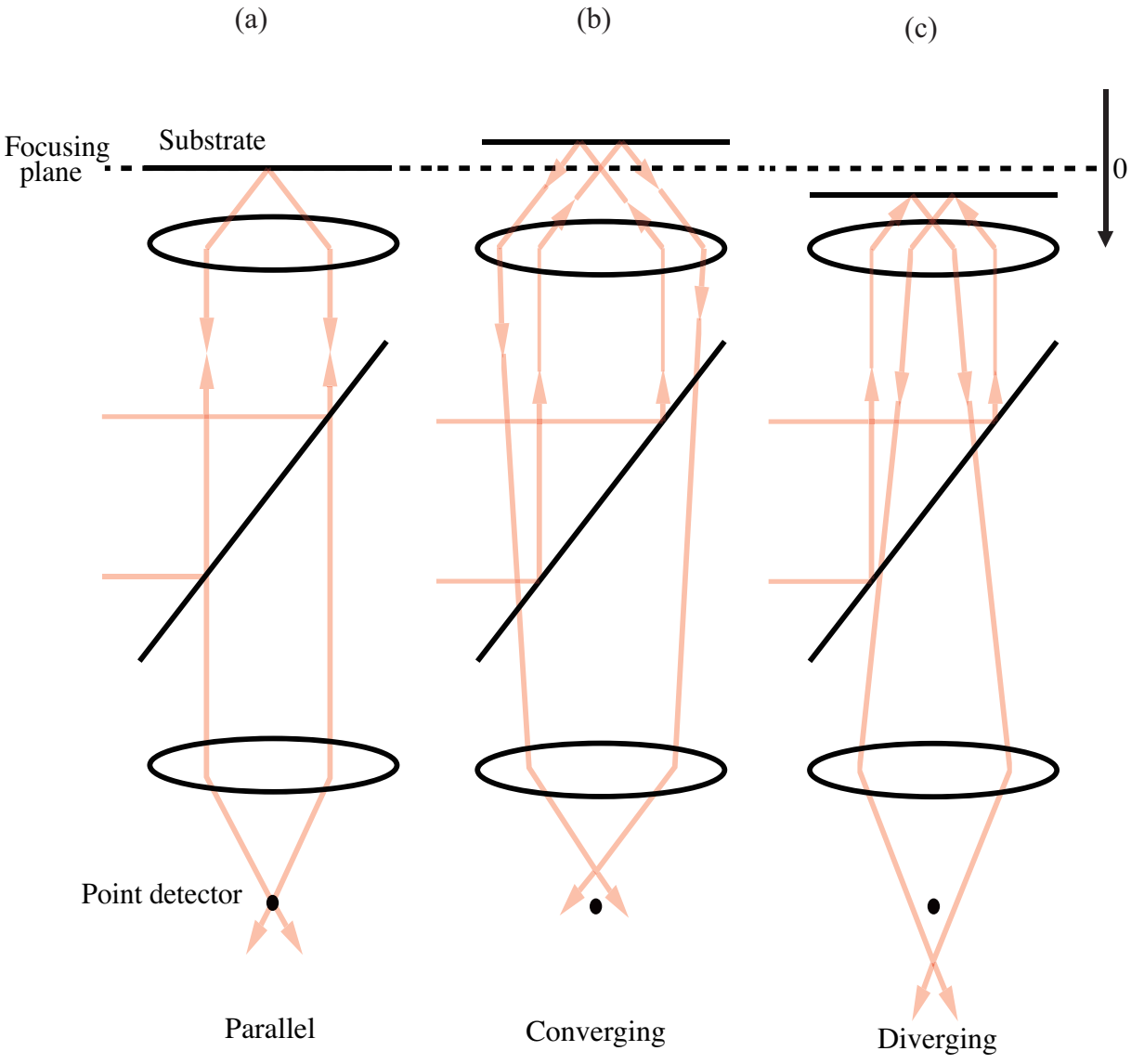


Fig. 28: Substrate correction by using a confocal optical system.

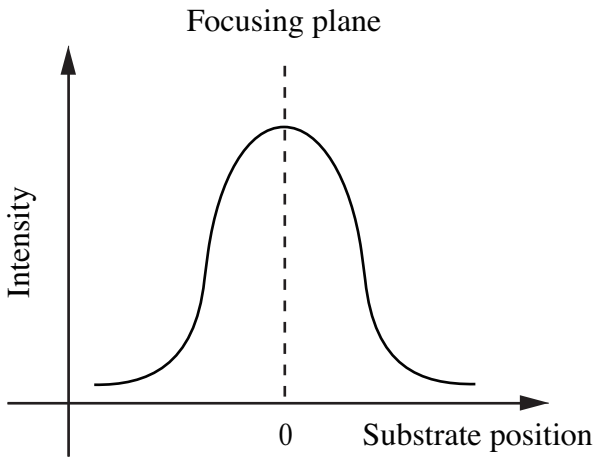


Fig. 29: Intensity variation regarding the position of the substrate.

Figure 30 shows an experimental result, in which pure water is injected and effective refractive index is measured under the substrate correction using the confocal method. One can see a very stable variation of effective refractive index. The averaged value of refractive index and standard deviation are 1.33000 and $6 \times 10^{-5}$, respectively. The measurement stability meets the requirement for virus detection.

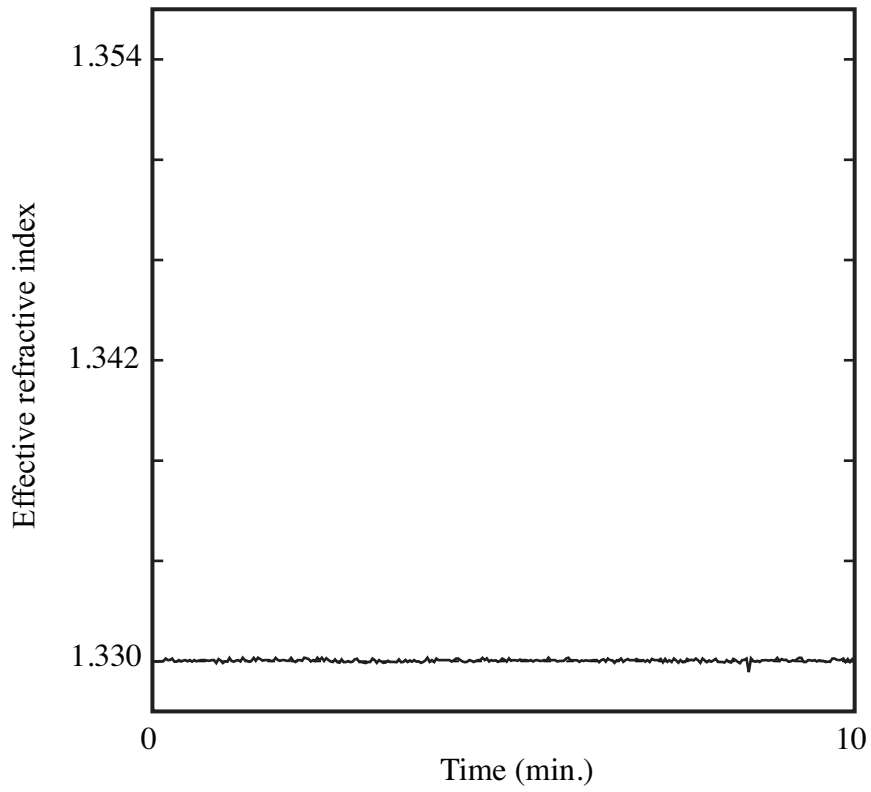


Fig. 30: Refractive variation under the correction of a substrate drift by confocal optical system.

## 4.2 Improvement of measurement stability after liquid exchange

Figure 31 shows the experimental result, in which pure water is injected per ∼10 minutes and effective refractive index was measured in the 45 minute. The vertical axis was calibrated by using pure water in the initial condition. One can see that there is a jump increase in the variation of effective refractive index after liquid exchange. In this experiment, a flow cell covered the substrate to supply the liquid to the sensing region, as shown in Fig. 32. The flow cell was produced by using the polydimethylsiloxane (PDMS) material by an optical method; the flow cell has a channel as a reservoir, as shown in Fig. 32. Pure water was pushed into the flow cell, and then pure water covered the sensing surface. If the size of a reservoir is too narrow, pressure of the injected liquid becomes high. Thus, a jump increase in effective refractive index appears. Consequently, larger reservoir is potentially contribute to stabilise the measurement of effective refractive index.

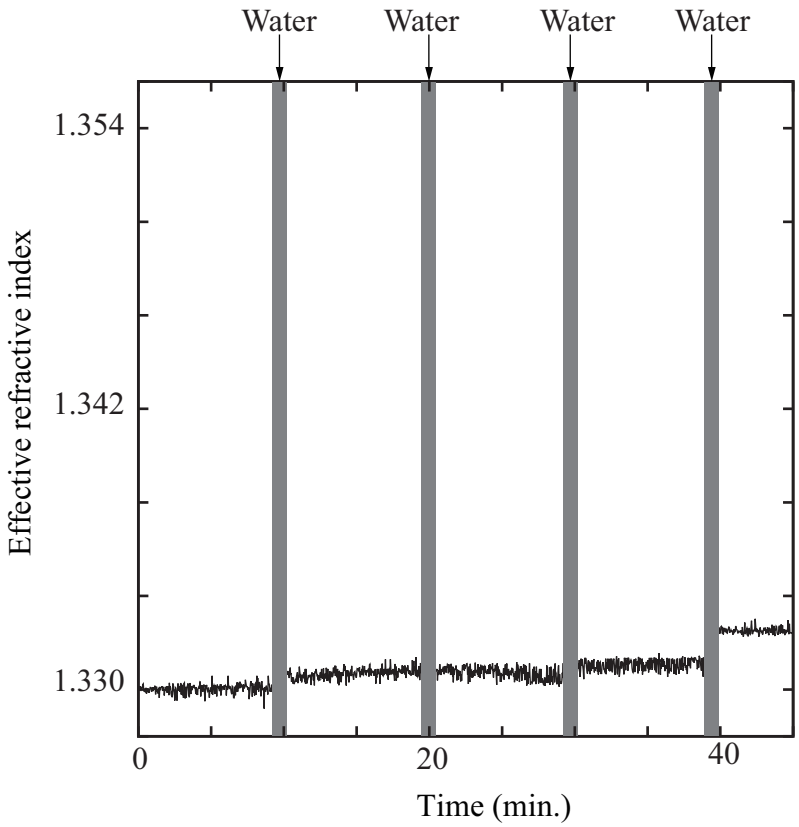


Fig. 31: Refractive index variation after liquid exchange.

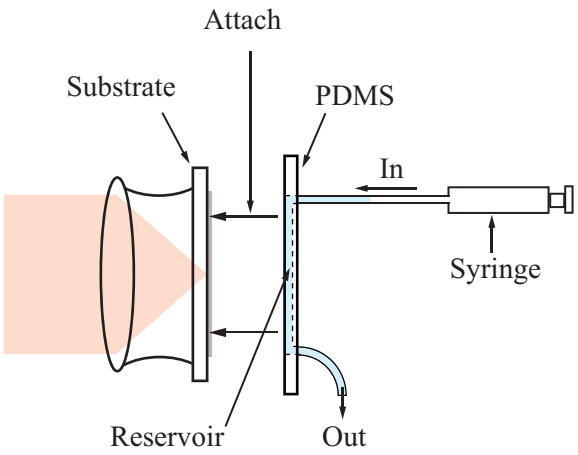


Fig. 32: PDMS flow cell covers the substrate to supply a liquid into the sensing region.

In order to avoid the influence of pressure increase, the flow cell was changed to the one shown in the Fig 33. The flow cell was produced by using a teflon material and a reservoir with $\sim 30$ $\mu$l by the mechanical fabrication.

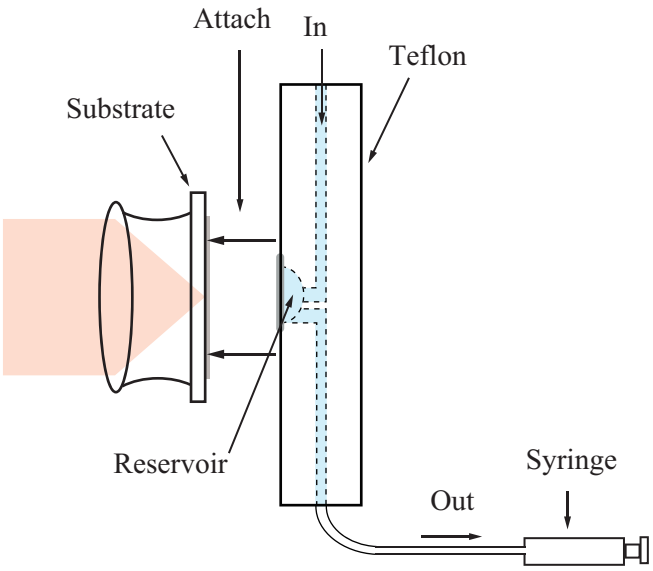


Fig. 33: Teflon flow cell covers the substrate to supply a liquid into the sensing region.

Figure 34 shows the variation of effective refractive index from 8 times injection of pure water in 45 minutes. Gray stripes indicate the timing of liquid injections. The vertical axis was calibrated by using pure water in the initial condition. One can see a stable variation of effective refractive index after liquid exchange. The averaged value and standard deviation are 1.3300 and $4 \times 10^{-4}$, respectively. The measurement stability meets the requirement for virus detection.

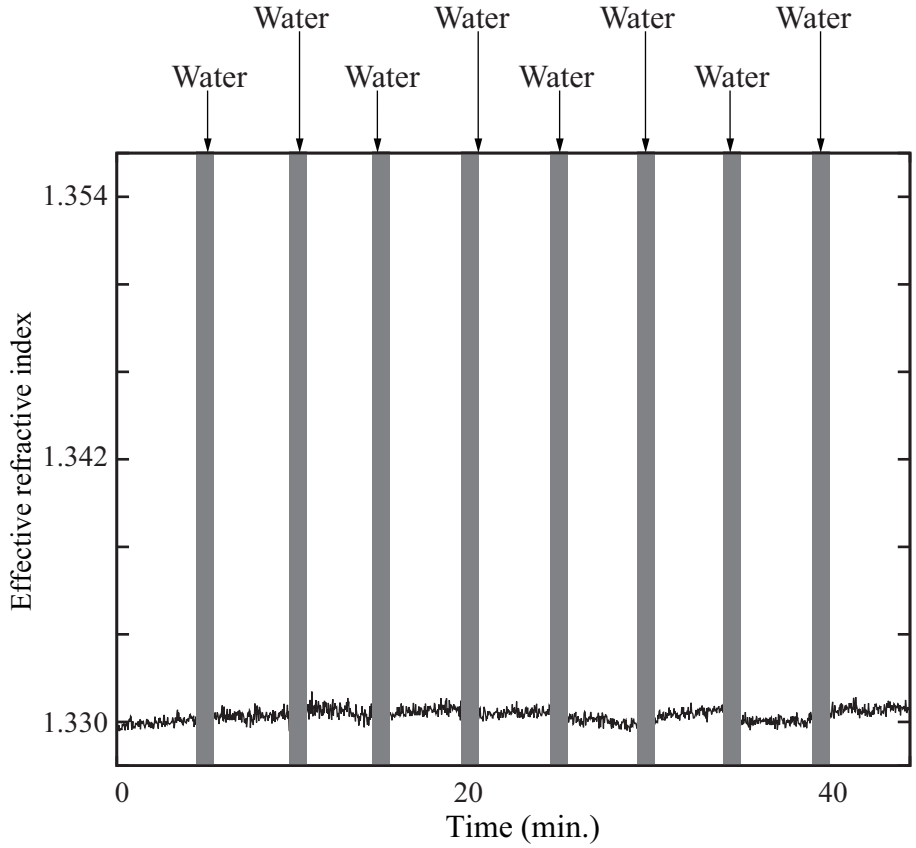


Fig. 34: Refractive index variation after liquid exchange in the teflon flow cell.

In the experiment for virus detection, different liquids are sequentially injected into the flow cell. In order to see influence of replacing the liquids, pure water and phosphate buffer saline (PBS, pH=6.1) were alternatively injected into the flow cell for a duration of $\sim 1$ hour. The experimental result is shown in Fig. 35. Injected liquid is shown at the top of the plot. The vertical axis was calibrated by using pure water in the initial condition. It can be seen that effective refractive index has a big change after PBS injection. I think that some volumes of liquid remained in the reservoir of the flow cell, which affected the value of effective refractive index of following liquids.

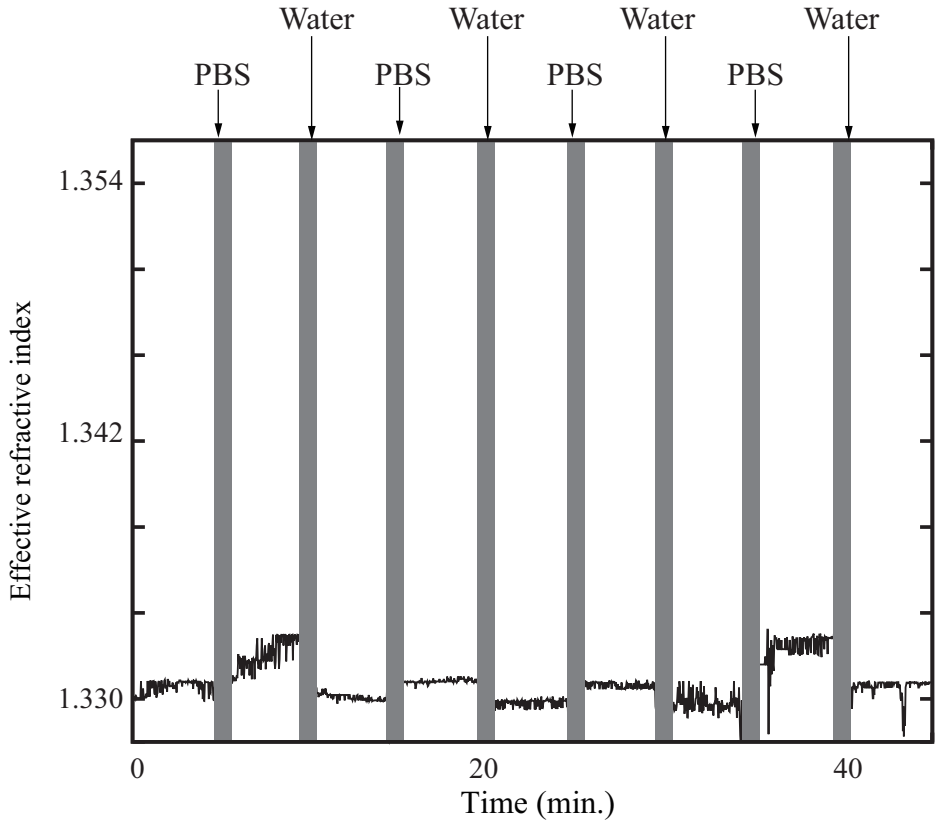


Fig. 35: Refractive index variation after liquid/PBS exchange in the teflon flow cell.

To resolve this problem, reservoir should be modified to straight-groove shape. Regarding the volume of the reservoir, it is difficult to produce the several $\mu$l by using the mechanical method. I selected a flow cell with combined PDMS and teflon components as shown in Fig. 36; it has a reservoir with $\sim$ 2.5 $\mu$l.

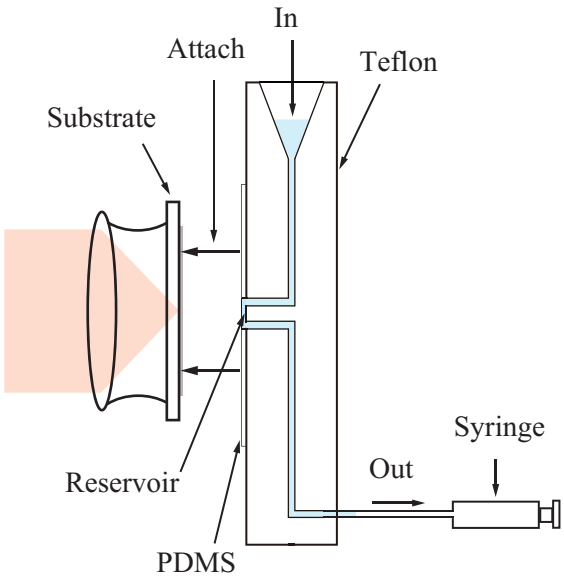


Fig. 36: A flow cell with combined teflon and PDMS components to supply a liquid into the reservoir.

Figure 37 shows the plot of refractive index variation by 8 times injections of pure water in the 45 minute time frame. The gray stripes indicate the timing of liquid injections in the plot. The average of effective refractive index and standard deviations are 1.3300 and $8 \times 10^{-5}$, respectively.

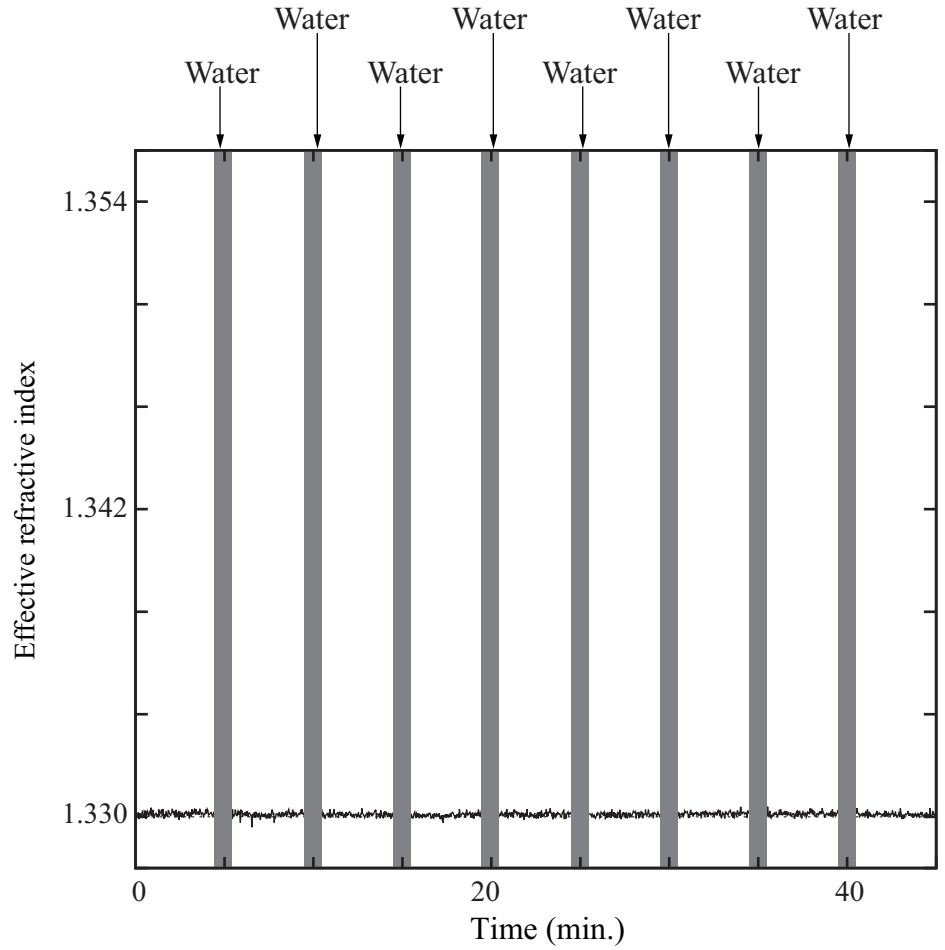


Fig. 37: Refractive index variation after injecting pure water 8 times in the 45 minute time frame.

Next, the pure water and PBS was alternately injected for 8 times in 45 minutes time frame. Figure 38 shows the measured effective refractive index versus time. The gray stripes indicate the timing of liquid injections. The vertical axis was calibrated by using pure water in the initial condition. The average of effective refractive indices for pure water and PBS are 1.3300 and 1.3318, respectively, and their standard deviations are $2 \times 10^{-4}$ and $4 \times 10^{-4}$, respectively. The measurement stability after liquids exchange meets the requirements for virus detection.

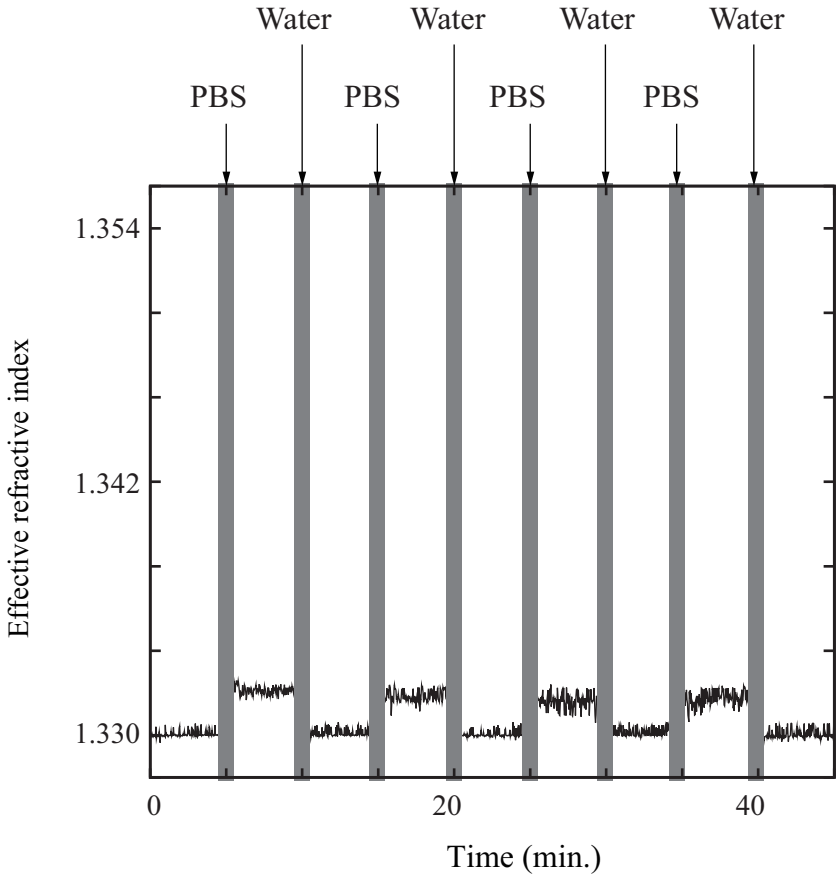


Fig. 38: Refractive index variation after alternatively injecting pure water and PBS.

# Chapter 5 Detection of influenza virus

A fast and highly sensitive method to determine subtypes of influenza viruses is important in medical institutes dealing with infectious diseases. In this chapter, a method based on localized surface plasmon sensor used to determine a subtype of influenza virus using antigen-antibody interactions is presented. In this method, variation of effective refractive index that arises from interactions between viruses and their monoclonal antibodies is measured in real time.

## 5.1 Preparation of influenza viruses and antibodies

### 5.1.1 Preparation of influenza viruses

For the detection of influenza viruses with specific subtypes, A/H1N1 and A/H3N2 viruses were employed, and they were prepared through the following processes. Influenza virus strain A/Puerto Rico/8/34 (A/PR8; A/H1N1) and A/Guizhou/54/89 (A/Guizhou; A/H3N2) were grown in the allantoic cavities of 10- to 11-day-old fertile chicken eggs. Each virus was purified from the allantoic fluids by differential centrifugation through a 10 to 50% sucrose density gradient and pelleted. The virus was resuspended in PBS and quantified by a BCA protein assay kit (Thermo Fisher Scientific, Yokohama, Japan) according to the manufacturer's instructions. The viral solution was diluted to 1 mg/ml of total protein and treated with 0.1% formalin at 4°C for a week to inactivate the virus.

### 5.1.2 Preparation of biotinylated monoclonal antibodies

In order to produce a surface that interacts against influenza viruses with certain subtypes, monoclonal antibodies were prepared. A hybridoma producing specific antibody against hemagglutinin (HA) of A/PR8 was propagated in serum-free Hybridoma-SFM media (Gibco, Tokyo, Japan) using a culture flask CELLine CL-1000 (BD Bioscience, San Jose, CA). A/PR8 HA-specific monoclonal antibodies were purified from culture supernatants by ammonium sulfate precipitation followed by affinity chromatography using rProtein A Sepharose Fast Flow (GE Healthcare, Tokyo, Japan) according to the manufacturer's instructions. The purified monoclonal antibodies were dialyzed against PBS, and the purity was determined by SDS-PAGE with Coomassie Brilliant Blue Staining. Biotinylation of this antibody was performed by the use of a Biotin Labeling Kit-NH2 (Dojindo, Mashiki, Kumamoto) according to the manufacturer's instructions.

## 5.2 Substrate fabrication

In order to produce a surface that interacts against influenza viruses with certain subtype, monoclonal antibodies are fixed on the surface. Figure 39 shows the structure of the sensing surface. On the gold surface of Kretschmann configuration described in the calculation part, avidin (Pierce Avidin 21121, Thermo Scientific, USA) molecules form a monomolecular layer by thiol binding, and biotinylated monoclonal antibodies cover the avidin layer by the avidin-biotin interactions.

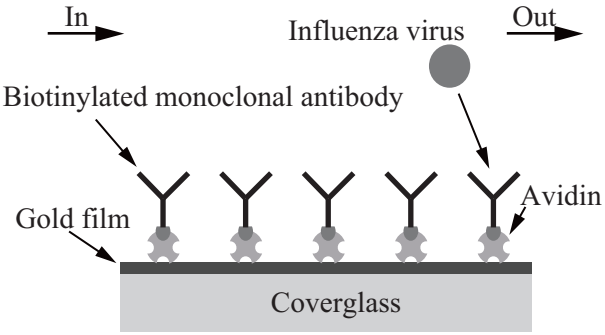


Fig. 39: Structure of the sensing surface for detecting influenza viruses with certain subtype. The surface of the gold film of Kretschmann configuration is covered with avidin molecules to hold biotinylated monoclonal antibodies.

To fabricate the surface of substrate, avidin dissolved in PBS (0.1 mg/ml) is injected into the flow cell, and then PBS is injected to discharge the free avidin molecules from the flow cell. Antibody dissolved in PBS (0.022 mg/ml) is also injected by the same procedure. The monoclonal antibodies for A/H1N1 virus are immobilized on the sensing surface. Effective refractive index on the gold surface is monitored during these procedures.

## 5.3 Optical setup for detecting the influenza virus with a specific subtype

Figure 40 shows the optical setup of a localized surface plasmon sensor. A He-Ne laser is used as a light source. The expanded laser beam with linear polarization passes through ZPol (Nanophoton, Japan) and is converted to quasi-radial polarization. The beam is focused on a gold film by an oil immersion objective lens. The reflected beam is collected by the same objective lens. To obtain spatial frequency distribution of the reflected beam, the exit pupil of the objective lens is imaged onto a CCD device. The spatial frequency distribution is analyzed to extract the propagating constant of excited localized surface plasmons, which is affected by the refractive index on the metal surface.

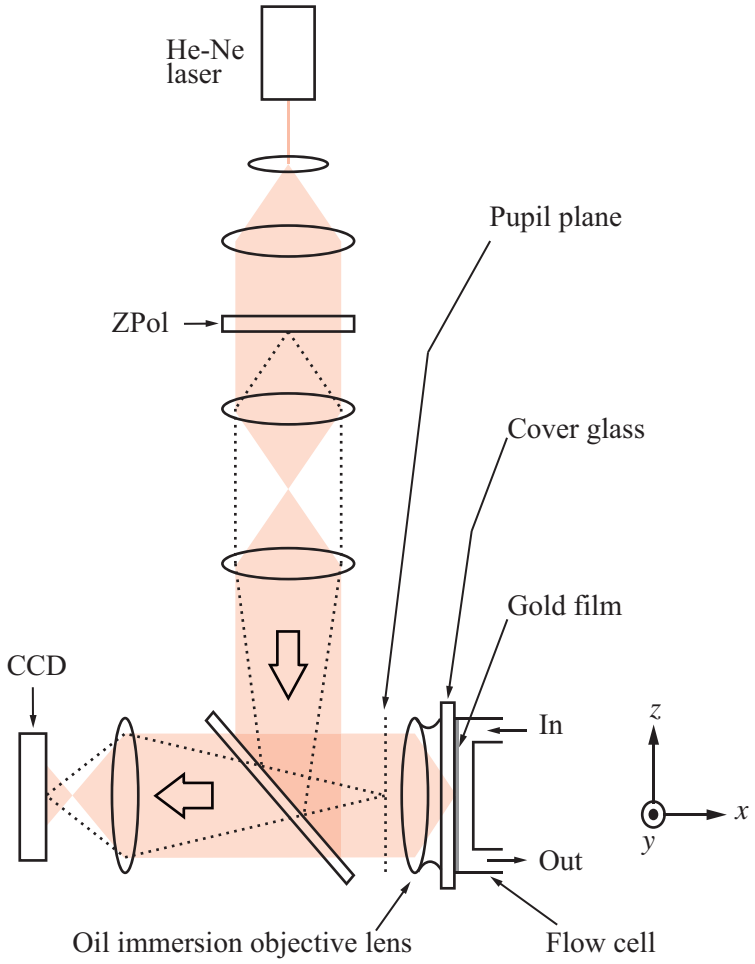


Fig. 40: Optical setup of the localized surface plasmon sensor.

## 5.4 Determination of influenza virus A/H1N1 from A/H3N2

Figure 41 shows variation of effective refractive index during an experiment on A/H1N1. In this experiment, the measurement started with pure water to calibrate the sensor, and then the substrate was fabricated against the H1N1 viruses after the injection of PBS. At the timing shown as gray stripes in Fig. 41, avidin and biotinylated antibodies were injected as described in the previous section. The volume of each injection was 100 $\mu$l. After discharging free antibodies from the flow cell, effective refractive index was measured as $\sim 1.3385$.

After the fabrication of sensing surface, A/H1N1 viruses (0.05 mg/ml) were injected with the volume of 100 $\mu$l. After the injection of viruses, one can see that the effective refractive index rapidly increased by $\sim$ 0.0115, which is $\sim$ 30 times larger than the standard deviation found in the experiment to clarify the sensor stability. It was also found that the effective refractive index saturates at the similar value in the several measurements under the same condition. Therefore, it can be supposed that the increase of effective refractive index arises from $\sim$ 7 viruses which bind at the sensing region.

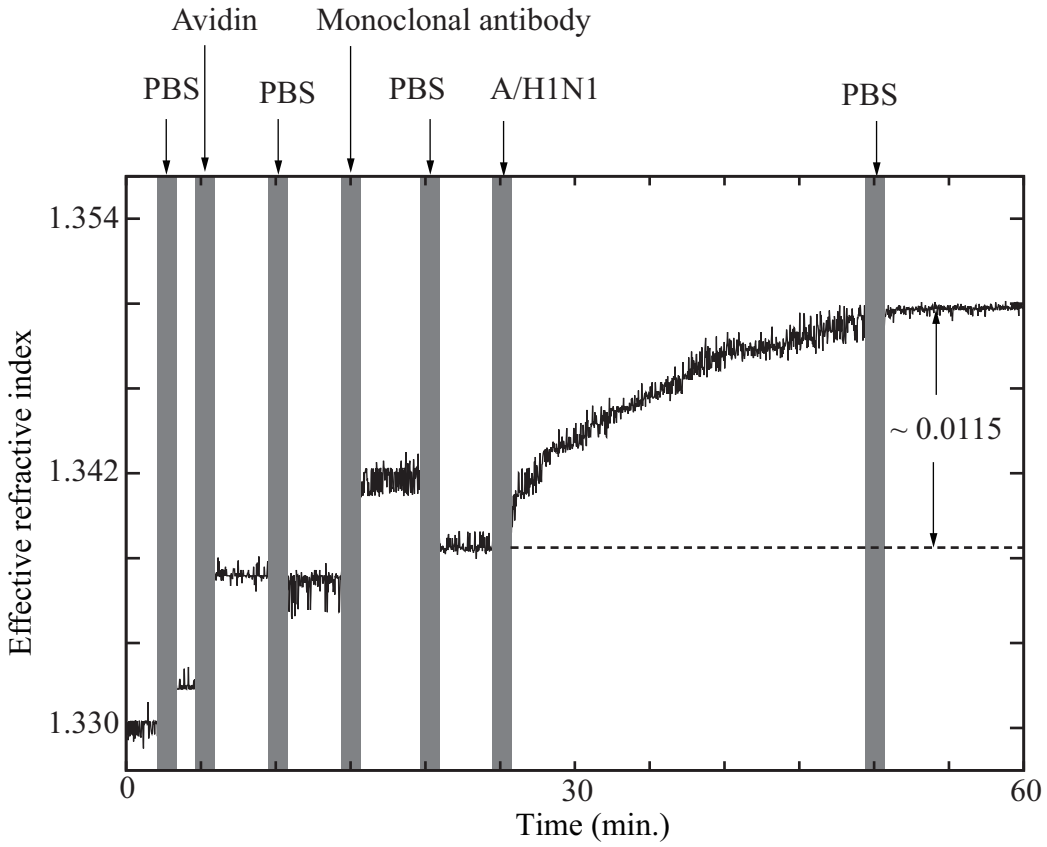


Fig. 41: Refractive index variation for the detection of H1N1 viruses.

Figure 42 shows an experiment on A/H3N2. The substrate was fabricated using the same procedures for the detection of H1N1 virus, and A/H3N2 viruses (0.05 mg/ml) were injected with the volume of 100 $\mu$l. One can see a smaller increase of refractive index than that of A/H1N1. After injecting PBS to exchange solution in the flow cell, refractive index returned to the value measured before the virus injection. From these experiments, it was confirmed that the sensor respondeds only to A/H1N1. Consequently, the developed sensor can be used to determine the subtypes of influenza viruses.

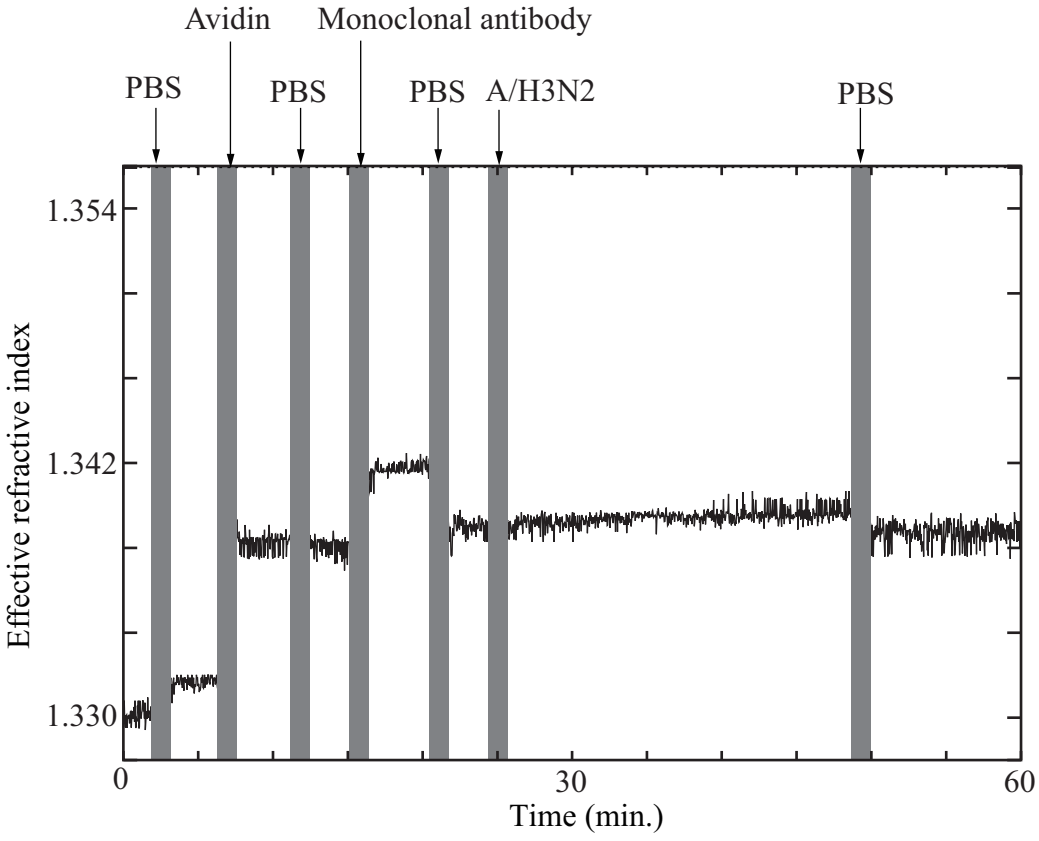


Fig. 42: Refractive index variation for the detection of H3N2 viruses.

# Chapter 6 Nasal swab specimen

Influenza viruses are a major cause of respiratory tract infection, which results in mortality and financial loss. Nevertheless, fast diagnosis of influenza viruses with specific subtypes has not been established yet. The fast diagnosis can improve medical management by allowing timely provision of antiviral therapy and prevention of infectious diseases. To evaluate the applicability of a localized surface plasmon sensor to diagnosis used in the real world, nasal secretions are collected from uninfected person; the secretions contained no influenza virus. Specimen prepared by nasal swab was measured to see influence from contamination. Details are presented in this chapter.

## 6.1 Preparation of a nasal swab specimen

The nasal swab is widely used in diagnosis of the influenza virus in clinics. A nasal swab specimen was prepared through the following processes. The nasal secretions were collected from an uninfected person as shown in Fig. 43 (a). A swab was gently inserted into the nostril straight back, along the floor of the nasal passage until reaching the the posterior wall of the nasopharynx. The swab was rotated several times, and withdrawn back from the nostril. To dilute the nasal secretions in the PBS, the swab is put into the tube having PBS with volume of 300 $\mu$l, as shown in Fig. 43 (b). After stirring the liquid with the swab several times, the swab was removed from the tube. The diluted nasal swab was centrifuged to exclude the some of the contaminants with large sizes, as shown in Fig. 43. Finally, the supernatant liquid was collected. The collected liquid was used as the nasal swab specimen and was applied in the experiment.

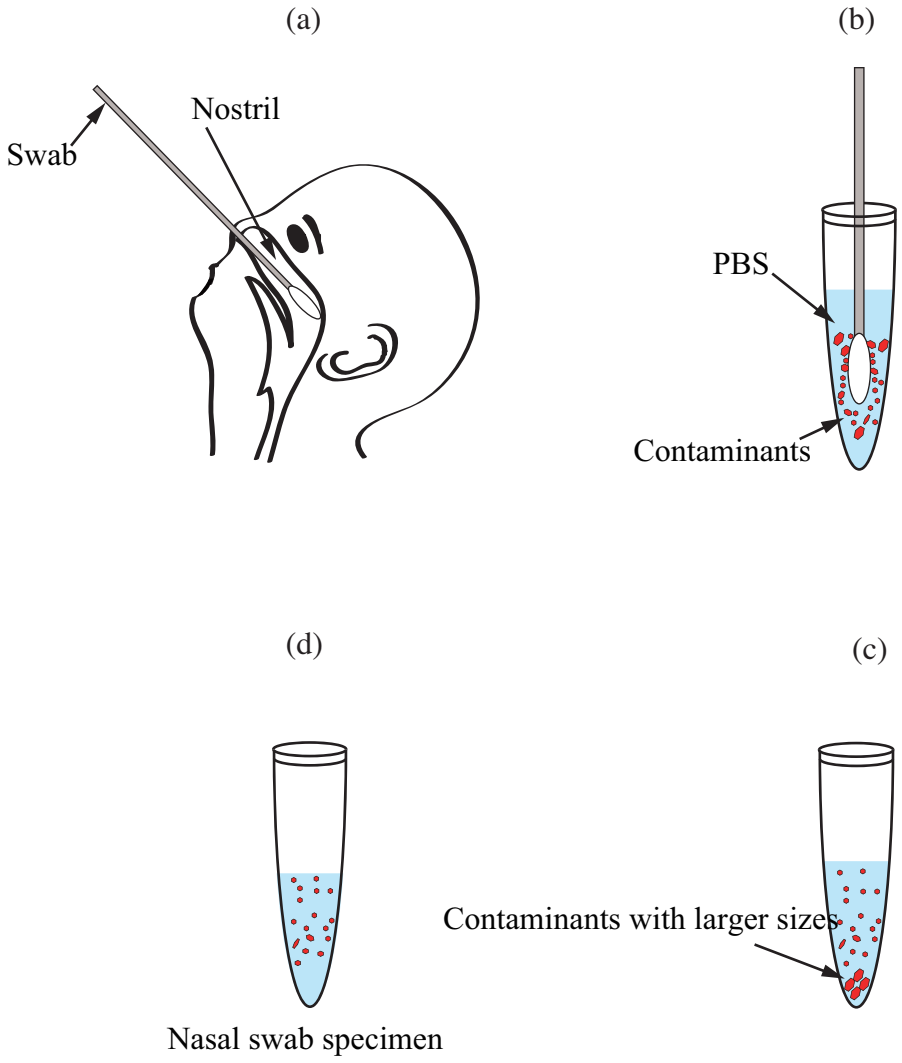


Fig. 43: Preparation processes of a nasal swab specimen.

## 6.2 Detection of a nasal swab specimen

The substrate was fabricated under the same condition as that of H1N1virus detection. Monoclonal antibodies for H1N1 virus were immobilized on the sensing surface. Figure 44 shows the variation of effective refractive index after injection the of nasal swab specimen. The measurement of effective refractive index started from pure water to calibrate the localized surface plasmon sensor, and then PBS was injected to start the substrate fabrication. After substate fabrication, the effective refractive index increased to ∼1.3382; this value is reliable. The nasal swab specimen with 100 $\mu$l was injected and followed the three times injection of PBS to exclude the contaminants from the sensing region. The effective refractive index increased at ∼0.002. The increased value after injection of H1N1 under the same condition is a factor of 6, comparing with that of the nasal swab specimen. If a nasal swab specimen contains influenza viruses with a specific subtype, it is possible to detected the viruses by using the proposed method.

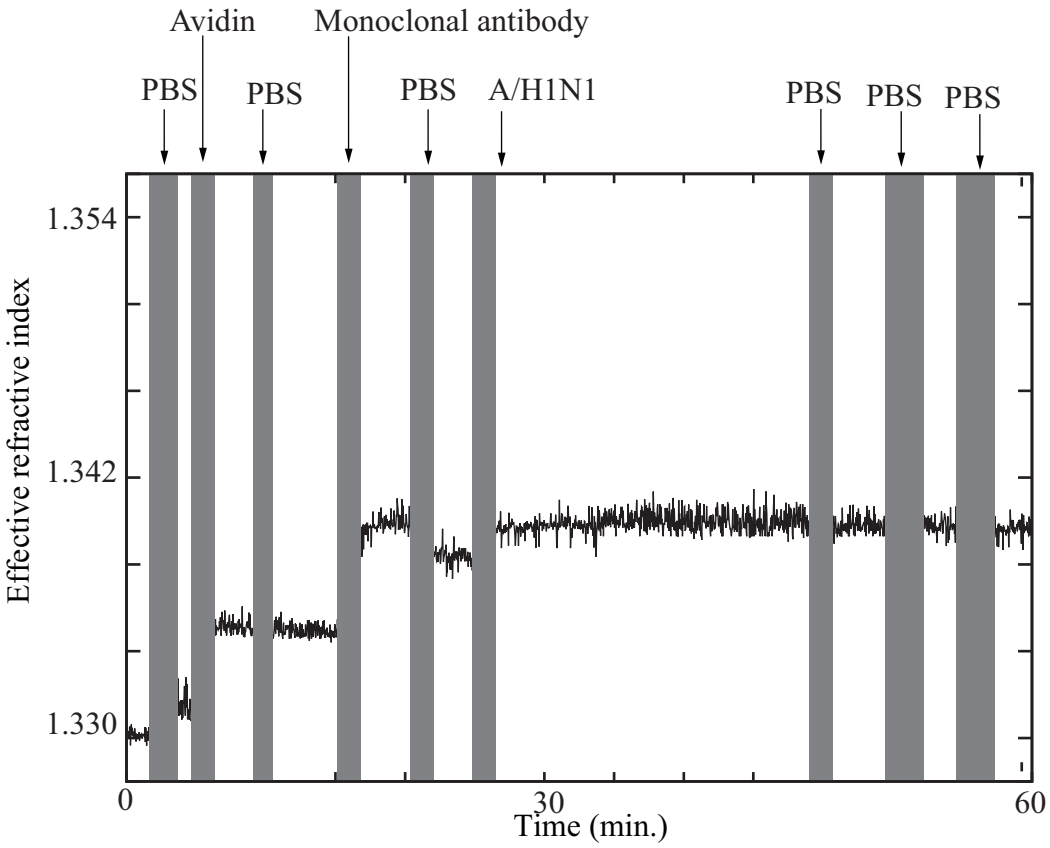


Fig. 44: Refractive index variation for evaluating the applicability of developed sensor to medical diagnosis.

# Chapter 7 Summary

In this thesis, I have proposed a bio-sensing method to detect influenza viruses with specific subtypes employing localized surface plasmons excited in the optical diffraction limit on a flat metal surface. In this method, localized surface plasmons are applied to measure the refractive index variation that arise from interactions between influenza viruses and their monoclonal antibodies which are immobilized on the metal surface. Potential developments in the near future are also considered. The calculation parameters are assumed according to real experiments for virus detection, and the theoretical calculated result has shown that the sensing volume of the localized surface plasmon sensor in this application is $\sim$ 6 al.

The measurement stability of the localized surface plasmon sensor has been improved to satisfy the requirements in the detection of influenza viruses by substrate correction and improvement of flow cell. Stability of refractive index in the order of $10^{-4}$ has been achieved in the measurement having liquid exchange processes.

The determination of the subtype of influenza virus has been demonstrated. In this demonstration, the monoclonal antibodies of A/H1N1 were immobilized on the sensing surface. The increase in effective refractive index arose from interactions between influenza viruses of A/H1N1 and the antibodies on the sensing surface. In the experiment, specific detection against A/H1N1 has also been also confirmed from A/H3N2 as a contrast sample. The response of the antigen-antibody interaction was measured at real-time. The influenza virus (A/H1N1) was rapidly identified by employing its monoclonal antibodies. It has been suggested that a localized surface plasmon sensor has the potential to detect a single influenza virus.

To evaluate the applicability of the developed sensor, a nasal swab specimen was prepared. In the experiment, substrates were fabricated under the same condition as that of A/H1N1 virus. The monoclonal antibodies for A/H1N1 virus were immobilized on the sensing surface. Effective refractive index on the gold surface was monitored during these procedures using the developed sensor. After injection of nasal swab specimen, the refractive index increased by $\sim$0.002. The increased value after injection of H1N1 is $\sim$6 times larger than that of the nasal swab specimen. The developed localized surface plasmon sensor was possible to determine influenza virus in the specimen prepared by using nasal swab.

# References


[1] H. Raether, *Surface plasmons on Smooth and Rough Surface and on gratings* (Springer-Verlag, Berlin, 1988).

[2] R. W. Wood, "On a remarkable case of uneven distribution of light in a diffraction grating spectrum," Proc. Phys. Soc. London **18**, 396-402 (1902).

[3] R. H. Ritchie, "Plasma losses by fast electrons in thin film," Phys. Rev. **106**, 874-881 (1957).

[4] A. Otto, "Excitation of nonradiative surface plasma waves in silver by the method of frustrated total reflection," Z. Phys. **216**, 398–410 (1968).

[5] E. Kretschmann and H. Reather, "Radiative decay of nonradiative surface plasmon excited by light," Z. Naturf. A **23**, 2135-2136 (1968).

[6] B. Liedberg, C. Nylander, and I. Lunström, "Surface plasmon resonance for gas detection and biosensing," Sens. Actu. **4**, 299–304 (1983).

[7] B. Rothenhausler and W. Knoll, "Surface plasmon microscopy," Nature **332**, 615–617 (1988).

[8] J. Homola, *Surface Plasmon Resonance Based Sensors, Springer Series on Chemical Sensors and Biosensors* (Springer-Verlag, Berlin, 2006).

[9] J. Homola, "Present and future of surface plasmon resonance biosensors," Anal. Bioanal. Chem. **377**, 528–539 (2003).

[10] A. Ramanavièius, F. W. Herberg, S. Hutschenreiter, B. Zimmermann, I. Lapënaitë, A. Kaušaitë, A. Finkelšteinas, and A. Ramanaviièienë, "Biomedical application of surface plasmon resonance biosensor (review)," Acta. Medica. Lituanica. **12**, 1–9 (2005).

[11] M. A. Cooper, "Label free screening of Bio-molecular interactions," Anal. Banal. Chem. **377**, 834–842 (2003).

[12] S. D. Soelberg, T. Chinowsky, G. Gelss, C. B. Soinelli, R. Stevens, S. Near, P. Kauffman, S. Yee, and C. E.Furlong "A portable surface plasmon resonance sensor system for real-time monitoring of small to large analytes ," J. Ind. Microbiol. Biotechnol. **32**, 669–674 (2005).

[13] P. M. Fratamico, T. P. Strobaugh, M. B. Medina, and A. G. Gehring, "Detection of escherichia coli O157:H7 using a surface plasmon resonance biosensor ," Biotechnology Techniques. **12**, 571–576 (1998).

[14] B. J. Luff, R. D. Harris, and J. S. Wilkinson, "Intergrated-optical directional coupler biosensor," Opt. Lett. **21**, 618–620 (1996).

[15] J. Homola, S. S. Yee, and G. Gauglitz, "Surface plasmon resonance sensor: review," Sensor and Actuators B-chem. **54**, 3–15 (1999).

[16] C. R. Shankaran, K. V. Gobi, and N. Miura, "Recent advancements in surface plasmon resonance immunosensors for detection of small molecules of biomedical, food and environmental interest," Sensor and Actuators B **121**, 158–177 (2007).

[17] H. Morgan and D. M. Taylor, "A surface plasmon resonance immunosensor based on the streptavidin-biotin complex," Biosens. Bielectron. **7**, 405–410 (1992).

[18] B. Liedberg, C. Nylander, and I. Lunström, " Biosensing with surface plasmon resonance-how it al started," Biosensor Bioelectron. **10**, i–ix (1995).

[19] W. M. Mullett, E. P. C. Lai, and J. m. Yeung, "Surface plasmon resonance-based immunoassays," Mehods. **22**, 77–91 (2000).

[20] M. Brigham-burke, J. R. Edwards, and D. J. O'Shannessy, "Detection of receptor-ligand interactions using surface plasmon resonance: model studies employing the HIV-1 gp120/CD4 interaction," Anal. Biochem. **205**, 125–131 (1992).

[21] E. De Genst, D. Areskoug, K. Decanniere, S. Muyldermans, and K. Andersson, "Surface plasmon resonance characterization of photoswitchable antigen-antibody interactions," Langmuir **15**, 3920–3923 (1999).

[22] H. J. Watts, D. Yeung, and H. Parkes, "Real time detection and quantification of DNA hybridization by an optical biosensor," Anal. Chem. **67**, 4283–4289 (1995).

[23] J. P. Jost, O. Munch, and T. Andersson, "Study of protein-DNA interaction by surface plasmon resonance (real time kinetics)," Nucl. Acids Res. **19**, 2788 (1991).

[24] F. C. Chien and S. J. Chen, "A sensitivity comparison of optical biosensors based on four different surface plasmon resonance mods," Biosens. Bioelectron. **20**, 633–642 (2004).

[25] X. Cui, F. Yang, Y. Sha, and X. Yang, "Real time immunoassay of ferritin using surface plasmon," Talanta **60**, 53–63 (2003).

[26] E. H. Gillis, J. P. Gosling, J. M. Sreenan, and M. Kane, "Development and validation of a biosensor-based immunoassay for progesterone," J. Immunol. Methods **267**, 131–138 (2002).

[27] H. Orelma, L. S. Johansson, I. Filpponen, O. J. Rojas, and J. Laine, "Generic method for attaching biomolecules via avidin-biotin complexes immobilized on films of regenerated and nanofibrillar cellulose," Biomacromolecules **13**, 2802–2810 (2012).

[28] J. Xu, J. Y. Wan, S. T. Yang, S. F. Zhang, N. Xu, N. Li, J. P. Li, H. Y. Wang, X. Bai, and W. S. Liu, " A surface plasmon resonance biosensor for direct detection of the rabies virus," Act. Vet. Brno. **81**, 107–111 (2012).

[29] H. Baac, J. P. Hajas, J. Lee, D. Kim, S. J. Kim, and M. L. Shuler, "Antibody based surface plasmon resonance detection of intact viral pathogen," Biotechnol. and Bioeng. **94**, 815–819 (2006).

[30] N. A. Cinel, S. Buton, and E. Ozbay, "Electron Beam Lithography designed silver nano disks as label free nano-biodensor based on localized surface plasmon resonance," Opt. Exp. **20**, 2587–2597 (2012).

[31] N. Mehan, V. Gupta, K. Sreenivas, and A. Mansingh, "Surface plasmon resonance based refractive index sensor for liquids," Indian Journal of Appl. Phys. **43**, 854–858 (2005).

[32] P. M. Boltovets, V. R. Boyko, I. Y. Kostikov, N. S. Dyacheko, B. A. Snopok, and Yu. M. Shirshov, "Simple method for plant virus detection: effect of antibody immobilization technique," J. Virol. Methods **105**, 141–146 (2002).

[33] D. K. Takemoto, J. J. Skehel, and D. C. Wiley, "A surface plasmon resonance assay for binding of influenza virus hemagglutinin to its sialic acid receptor," Virology **217**, 452–458 (1996).

[34] R. J. Green, R. A. Frazier, K. M. Shakesheff, M. C. Davies, C. J. Roberts, and S. J. B. Tendler, "Surface plasmon resonance analysis of dynamic biological interactions with biomaterils," Biomaterials **21**, 1823–1835 (2000).

[35] H. Knobloch, H. Orendi, M. Buchel, M. Sawodny, A. Schmidt, and W. Knoll, "Optical switching of azobenzene sidechain molecules observed by surface plasmon spectroscopy," Fresenius J. Anal. Chem. **349**, 107–111 (1994).

[36] J. Homola, "Surface plasmon resonance sensors for detection of chemical and biological species," Chem. Rev. **108**, 462–493 (2008).

[37] C. E. Jordan, A. G. Frutos, A. J. Thiel, and R. M. Corn, "surface plasmon resonance imaging measurements of DNA hybridization adsorption and streptavidin/DNA multilayer formation at chemically modified gold surfaces" Anal. Chem. **69**, 4939–4947 (1997).

[38] M. Piliarik and J. Homola, "Surface plasmon resonance (SPR) sensor: approaching their limits?," Opt. Exp. **19**, 16505–16517 (2009).

[39] R. Slavik and J. Homola, "Ultrahigh resolution long range surface plasmon-based sensor,'" Sensors and Actuators B **123**, 10–12 (2007).

[40] H. Kano, S. Mizuguchi, and S. Kawata, "Excitation of surface-plasmon polaritons by a focused laser beam," J. Opt. Soc. Am. B **15**, 1381–1386 (1998).

[41] H. Kano and W. Knoll, "Locally excited surface-plasmon-polaritons for thickness measurement of LBK film," Opt. Commun. **153**, 235–239 (1998).

[42] H. Kano and W. Knoll, "A scanning microscope employing localized surface-plasmon-polaritons as a sensing probe," Opt. Commun. **182**, 11–15 (2000).

[43] K. Watanabe, N. Horiguchi, and H. Kano, "Optimized measurement probe of the localized surface palsmon microscope by using radially polarized illumination," Appl. Opt. **46**, 4985–4990 (2007).

[44] E. N. Economou, "Surface plasmons in thin films," Phys. Rev. **182**, 539–554 (1969).

[45] A. Bressoud, J. Whitcomb, C. Pourzand, O. Haller, and P. Cerutti, "Rapid detection of influenza virus H1 by the polymerase chain reaction," Biochem. Biophys. Res. Commun. **167**, 425–430 (1990).

[46] R. A. M. Fouchier, T. M. Bestebroer, S. Herfst, L. V. D. Kemp, G. F. Rimmelzwaan, and A. D. M. E. Osterhaus, "detection of influenza A viruses from different species by PCR amplification of conserved sequences in the matrix gene," J. Clin. Microbiol. **38**, 4096–40101 (2000).

[47] J. S. Ellis and M. C. Zambon, "Molecular diagnosis of influenza" Rev. Med. Virol. **12**, 357–389 (2002).

[48] D. Lepage, A. Jiménez, J. Beauvais, and J. J. Dubowski, "Real-time detection of influenza A virus using semiconductor nanophotonics," Light:Science and Application. **2**, 1–8 (2013).

[49] M. Petric, L. Comanor, and C. A. Petti, "Role of the laboratory in diagnosis of influenza dying seasonal epidemics and potential pandemics," J. Infect. Dis. **194**, 98–110 (2006).

[50] D. Dwyer, D. W. Smith, M. G. Catton, and I. G. Barr, "Laboratory diagnosis of human seasonal and pandemic influenza virus infection," Medical Journal of Australia **185**, S48–53 (2006).

[51] T. Chou, W. Hsu, C. Wang, Y. Chen, and J. Fang, "Rapid and specific influenza virus detection by functionalized magnetic nano particles and mass spectrometry," J. Nanobiotechnology **9**, 1–13 (2011).

[52] P. J. Gavin and R. B. Thomson Jr, "Review of Rapid diagnostic test for influenza," Clin. applied I mmunol. Rev. **4**, 151–171 (2003).

[53] A. Yamada, J. Imanishi, E. Nakajima, K. Nakajima, and S. Nakanima, "Detection of influenza viruses in throat swabs by using polymerase chain reaction," Microbiol. Immunol. **35**, 259–265 (1991).

[54] M. Panning, M. Eickmann, O, Landt, M. Monazahian, S. Ölschläger, S. Baumgarte, U. Reischl, J. J. Wenzel, H. H. Niller, S. Günther, B. Hollmann, D Huzly, J. F. Drexler, A. Helmer, S. Becker, B. Matz, A. M. Eis-Hübinger, and C. Drosten, "Detection of influenza A(H1N1) virus by real-time PT-PCR," Eurosurveillance **14**, 1–6 (2009).

[55] Z. Rani and I. Hussain, "Immunofluorescence in immunobullous disease," Journal of Pakistan Association of Dermatologists **13**, 76–88 (2003).

[56] D. E. Noyola, B. Clark, F. T. O窶冩onnell, R. L. Atmar, J. Greer, and G. J. Demmler, "Comparison of a new neuraminidase detection assay with an enzyme immunoassay, Immunofluorescence, and culture for rapid detection of Influenza A and B Virues in Nasal Wash Specimens," J. Clin. Microbiol. **38**, 1161–1165 (2000).

[57] M. Svedendahl, S. Chen, A. Dmitriev, and M. Käll, "Refractometric sensing using propagating versus localizes surface plasmons: A Direct Comparison," Nano Lett. **9**, 4428–4433 (2009).

[58] E. M. Yeatman, "Resolution and sensitivity in surface plasmon microscopy and sensing," Biosensor and Bioelectronics **11**, 635–649 (1996).

[59] C. Huang, K. Bonoroy, G. Rreekman, and K. Verstreken. "An on chip localized surface plasmon resonance-based biosensor for label free monitoring of antige-antibody reaction," Microeletronic Eng. **86**, 2437–2441 (2009).

[60] D. Dry and T. Goswami, "Optical Biosensors: A Revolution Towards Quantum Nanoscale Electronics Device Fabrication," J. Biomed. and Biotechnol. **2011**, 1–7 (2011).

[61] X. Fan, I. M. White, S. I. Shopova, H. Zhu, J. D. Suter, and Y. Sun, "Sensitive optical biosensors for unlabeled target: A review," Analytica chimica. Acts. **620**, 8–26 (2008).

[62] Z. Yu and S. Fan, "Extrordinartily high spectral sensitivity in refractive index sensor using multiple optical modes," Opt. Exp. **19**, 10029–10040 (2011).

[63] S. Roh, T. Chung, and B. Lee, "Overview of the characteristics of micro and nano structured surface plasmon resonance sensors," Sensors. **11**, 1565–1588 (2011).

[64] J. G. Quinn, A. O. Neill, A. Doyle, C. M. Atamney, D. Diamond, B. D. Maccrainth, and R. O. Kennedy, " Development and application of surface plasmon resonance-based biosensors for the detection of cell-ligand interctions," Anal. Biochem. **281**, 135–143 (2000).

[65] Y. C. Kuo, J. H. Ho, T. J. Yen, H. F. Chen, and O. K. Lee, "Development of a surface plasmon resonance biosensor for real-time detection of osteogenic differentiation in live mesenchymal stem cell," PLos one **6**, e22382 (2011).

[66] S. Ekgasit, C. Thammacharoen, F. Yu, and W. Knoll, "Influenza of the metal film thickness on the sensitivity of surface plasmon resonance biosensors," Appl. Spectroscopy **59**, 661– 667 (2005).

[67] W. L. Bares, A. Dereux, and T. W. Ebbescen, "Surface plasmon subwavelenegth opticas," Nature **424**, 824–830 (2003).

[68] X. D. Hoa, A. G. Kirk, and M. Tabrizian, "Toward integrated and sensitive surface plasmon resonance biosensors: a review of recent progress," Biosensor Bioelectron. **23**, 151–160 (2007).

[69] P. Englebienne, A. V. Hoonacker, and M. Verhas, "Surface plasmon resonance: principles, methods and applications in biomedical sciences" Spectroscopy. **17**, 255–273 (2003).

[70] V. Kodoyianni, "Label free analysis of bimolecular interactions using SPR imaging," BioTechniques. **50**, 32–40 (2011).

[71] Y. Chen and H. Ming, "Review of surface plasmon resonance and localized surface plasmon resonance sensor," Photonic sensor. **2**, 37–49 (2012).

[72] H. Kano and S. Kawata, "Grating-coupled surface plasmon for measuring the refractive index of a liquid sample," Jpn. J. Appl. Phys. **34**, 331–335 (1995).

[73] S. A. A. Oloomi, A. Saboonchi, and A. Sedaghat, "Effects of thin film thickness on emittance, reflectance and transmittance of nanao scale multilayers," Int. J. Phys. Sci. **5**, 465–469 (2010).

[74] J. M. Pitarke, V. M. Silkin, E. V. Chulkov, and P. M. Echenique, "Theory of surface plasmons and surface plasmon polaritons," Rep. Prog. Phys. **70**, 1–87 (2007).

[75] S. Cagnin, M. Caraballo, C. Guiducci, P. Martini. M. Ross. M. Santaana, D. Danley, T. West, and G. Lanfranchi, "Overview of Electrochemical DNA Biosensors: New Approaches to Detect the Expression of Life," J. **9**, 3122–3148 (2009).

[76] K. Watanabe, G. Terakado, and H. Kano, "Localized surface plasmon microscope with an illumination system employing a radially polarized zeroth-order Bessel Beams," Opt. Lett. **34**, 1180–1182 (2009).

[77] G. Terakado, K. Watanabe, and H. Kano, "Scanning confocal total internal reflection fluorescence microscopy by using redial polarization in the illumination system," Appl. Opt. **48**, 1114–1118 (2009).

[78] K. Watanabe, M. Ryosuke, G. Terakado, T. Okazaki, K. Morigaki, and H. Kano, "High resolution imaging of patterned model biological membranes by localized surface plasmon microscopy," Appl. Opt. **49**, 887–891 (2010).

[79] L. G. Schulz, "The optical constants of silver, gold, copper, and aluminum. ll. The index of refraction n," J. Opt. Soc. Am. **44**, 362–367 (1954).

[80] L. G. Schulz and F. R. Tangherlini, "Optical properties of thin films of cadmium sulfide," J. Opt. Soc. Am. **44**, 368–370 (1954).

[81] K. Watanabe, K. Matsuura, F. Kawata, K. Nagata, J. Ning, and H. Kano, "Scanning and non-scaning surface plasmon microscopy to observe cell adhesion sites," Biomed. Opt. Express. **3**, 354–359 (2012).

[82] K. Watanabe, R. Miyazaki, G. Terakado, T. Okazaki, K. Morigaki, and H. Kano, "Localized surface plasmon microscopy of submicron domain structures of mixed lipid bilayers," Biomed. Opt. Express. **3**, 2012–2020 (2012).

[83] C.Wittekindt, B. Fleckenstein, K. Wiesmuller, B. R.Eing, and J. E. Kuhn, "Detection of human serum antibodies against type-specifically reactive peptides from the N-terminus of glycoprotein B of herpes simplex virus type 1 and type 2 by surface plasmon resonance," J. Virol. Methods **87**, 133–144 (2000).

[84] H. Bai, R. Wang, B. Hargis, H. Lu, and Y. Li, "A SPR aptasensor for detection of avian influenza virus H5N1," Sensor **12**, 12506–12518 (2012).

[85] L. C. Su, C. M. Chang, Y. L. Tseng, Y. F. Chang, Y. C. Li, Y. S. Chang, and C. Chou, "Rapid and highly sesitive method for influenza A (H1N1) virus detection," Anal. Chem. **84**, 3914–3920 (2012).

[86] C. Mandenius, R. Wang, A. Aldon, G. Bergstrum, S. Thobault, C. Lutsch, and S. Ohlson, "Monitoring of influenza virus hemagglutinin in process samples using week affinity ligands and surface plasmon resonance," Anal. Chim. Acta **628**, 66–75 (2008).

[87] P. M. Boltovets, B. A. Snopok, V. R. Boyko, T.P. Shevchenko, N. P. Shevchenko, N. S. Dyachenko, Yu. M. Shirshov, "Detection of plant viruses using a surface plasmon resonance via complexing with specific antibodies," J. Virol. Methods **121**, 101–106 (2004).